DEMOCRATIC AND POPULAR REPUBLIC OF ALGERIA
MINISTRY OF HIGH EDUCATION AND SCIENTIFIC RESEARCH
UNIVERSITY OF MOHAMED BOUDIAF - M'SILA

FACULTY OF SCIENCES
DEPARTMENT OF PHYSICS
N°: PH/MAT/07/2025

DOMAINE: SCIENCE OF MATIER
FIELD: PHYSICS
OPTION: MATERIAL PHYSICS

Memory Submitted for Obtaining
Diploma of Academic Master
Prepared by: Ali Saoucha Abdellah

TITLE :

Electronic band structure and optical characteristics of new lead-free halide perovskites for solar cell applications based on DFT

Defended on: 18/06/2025 before the jury composed of:

Dr. Saber Saad Essaoud	**University of Msila**	**Chairman**
Dr. Djamel Allali	**University of Msila**	**Supervisor**
Dr. Rabie Amari	**University of Msila**	**Assistant Supervisor**
Dr. Ammar Boukhari	**University of Msila**	**Examiner**
Dr. Elhadj Benrezgua	**University of Msila**	**Examiner**

Academic Year: 2024/2025

Acknowledgements

• *First and foremost, I thank **ALLAH**, the Almighty, who*

granted me health, courage, patience, and willpower, enabling me to carry out and complete this work.

• *I also thank my supervisor, **Djamel ALLALI**, for guiding me and for his valuable advice, which was of great help in writing this thesis.*

• *I would like to thank all the members of the jury, Mr. **Saber Saad Essaoud**, Mr. **Rabie Amari**, Mr. **Ammar Boukhari** and Mr. **Elhadj Benrezgua** at the University of Mohamed Boudiaf of M'sila.*

Dedication

I dedicate this work to:

- *All my **classmates** who studied with me during the 2024/2025 school year.*
- *My **dear parents**, my **wife**, and my **children**.*

ملخص

لقد قمنا في هذه المذكرة بدراسة الخواص البنيوية، الالكترونية، الضوئية، للمركبات **$AgCaBr_3$**،**$AgSrBr_3$** و **$AgBaBr_3$** ، باستعمال طريقة الأمواج المستوية مع الكمون الزائف في إطار نظرية دالية الكثافة الالكترونية**(DFT)** ، المدمجة في برنامج **CASTEP**. لقد استعملنا تقريب التدرج المعمم **(GGA-PBEsol)** لمعالجة كمون تبادل – ارتباط (XC) من أجل حساب الخواص البنيوية وتقريب **HSE06** و **TB-mBJ** من أجل حساب الخواص الالكترونية و الضوئية .

يمكن تلخيص النتائج المتحصل عليها فيمايلي:

•هناك توافق جيد بين نتائج حسابات المعاملات البنيوية(ثوابت الشبكة البلورية، معامل الانضغاط ***B*** ومشتق معامل الانضغاط ***B´*** للحالة الأساسية مع النتائج النظرية المتوفرة في المنشورات العلمية.

•بينت نتائج الحسابات أن المواد المدروسة تنتمي لعائلة أنصاف النواقل بموانع طاقة أساسية غيرمباشرة R–Γ .

•تم حساب الجزء التخيلي $\varepsilon_2(\omega)$ والجزء الحقيقي $\varepsilon_1(\omega)$ لدالة السماحية $\varepsilon(\omega)$ ،الإنعكاسية $R(\omega)$ ،قرينة الإنكسار $n(\omega)$ ،معامل الخمود $K(\omega)$ ،دالة ضياع الطاقة الإلكترونية $L(\omega)$ ومعامل الإمتصاص $\alpha(\omega)$ في مجال طاقوي من 0 إلى 30 إلكترون فولط (eV).

Abstract

In this study, we investigated the structural, electronic, and optical properties of the compounds $AgCaBr_3$, $AgSrBr_3$, and $AgBaBr_3$ using the plane-wave pseudopotential method within the framework of density functional theory (DFT), as implemented in the CASTEP code. The generalized gradient approximation (GGA-PBEsol) was used to treat the exchange-correlation potential for calculating the structural properties, while the HSE06 and TB-mBJ approximations were employed to evaluate the electronic and optical properties.

The main results obtained can be summarized as follows:

• There is a good agreement between the calculated structural parameters (lattice constants, bulk modulus, and its pressure derivative) in the ground state and the theoretical results reported in the literature.

• The electronic calculations show that the studied materials belong to the semiconductor family with indirect band gaps of the R–Γ type.

• The imaginary and real parts of the dielectric function, reflectivity, refractive index, extinction coefficient, electron energy loss function, and absorption coefficient were calculated in the energy range from 0 to 30 eV.

Nomenclature

Frequently used abbreviations:

DFT	Density Functional Theory
H	Hartree**.**
HF	Hartree-Fock.
Xc	Exchange Correlation.
KS	Kohn-Sham.
LDA	Local Density Approximation.
LSDA	Local Spin Density Approximation.
GGA	Generalized Gradient Approximation.
PBEsol	Perdew-Burke-Ernzerhof functional for Solids.
TB-mBJ	Tran-Blaha modified Becke-Johnson potential.
PP-PW	Pseudopotential-Plane Wave.
ZB	Brillouin Zone.
AE	All Electrons.
NC	Norm-Conserving.
BHS	Bachelet, Hamann, Schlüter procedure for constructing norm- conserving PP.
KB	Kleinman and Bylander**.**
US-PP	Ultrasoft pseudopotential**.**
APW	Augmented Plane Wave.
LAPW	Linearized Augmented Plane Wave.
FP	Full Potential.
MT	Muffin-Tin region.
I	Interstitial region.
LO	Local Orbitals.
EOS	Equation Of State.
BM	Birch Murnaghan.
V-R-H	Voigt-Reuss-Hill.
Eg	Energy band gap.
VB	Valence Band.
CB	Conduction Band.
TDOS	Total Density Of States.
PDOS	Partial Density Of States.

Contents

GENERAL INTRODUCTION

General Introduction

One of the most advantageous and easiest ways of predicting new materials is ab initio calculations (i.e. the first principles). The term ab initio is Latin for "from the beginning". This name is given to calculations derived directly from theoretical principles without the inclusion of experimental data. The materials are composed of atoms as building units. The atoms themselves are made up of electrons. The idea behind the first principles is to apply the fundamental laws of physics to identify the behavior of a material by performing electronic structure calculations.

The so-called ab initio methods for electronic structure calculations are widely used in modern science. They allow us to simulate and sometimes even predict the properties of actual materials without using adjustable parameters. These methods require practically no information about the system; it is necessary to use only atomic numbers and coordinates as input to start the calculation. Then, all the properties of materials such as cohesive energy, equilibrium crystalline structure, phase transitions, transport properties, magnetism, ferroelectricity, optical properties and others can be extracted from the calculation and sometimes directly compared to experimental data.

The ab initio study was only relatively recently possible with the development of reliable computer algorithms and the availability of high-performance parallel computing facilities. Ab initio calculations can be done now on systems that only a few years ago could only be processed with semi-empirical or empirical methods.

Inorganic halide perovskites have garnered significant attention due to their unique properties and their implication in diverse applications. The recent integration of ABX_3 halide perovskite materials as photoabsorbers has revolutionized photovoltaic solar cells, leading to a remarkable increase in power conversion efficiency from approximately 3.8% in 2009 to nearly 25% in 2019 [1–5]. Moreover, the applications of these materials extend beyond photovoltaics; they are also exploited in photodetectors, batteries and LEDs [6,7]. The flexibility of perovskites in terms of composition allows for the creation of a wide range of new structures. This versatility gives rise to a broad spectrum of novel chemical and physical properties [8], rendering them a highly significant category of functional materials. These materials have been extensively studied and applied in numerous fields, including ferroelectricity [9–12], piezoelectricity [9,13], ceramic science [14,15], photovoltaics [3,16–19]

One of the most ranges of these materials is the halide perovskites ABX_3, where X represents halides like F, Cl, Br, or I. These compounds have attracted significant attention in the fields of technology and science because of their exceptional optical, electrical, and

magnetic properties, as well as their cost-effective manufacturing process [8,16,20–25]. They are increasingly being utilized in solar cells, optical fibers, solid-state lubricants, thin-film electrolytes, lasers, thermoelectrics, and other applications that exploit their piezoelectric, optoelectronic, photochemical, and photoluminescent properties [24,26–33].

In recent work, Gómez-Peralta and Bokhimi [34] employed Artificial Neural Networks (ANN) [35] to predict the properties of a series of halide perovskites. The AgXBr3compounds, where X are Ca, Sr, or Ba, are among the aforementioned predicted halide perovskites. These three compounds have been predicted to crystalize in their idealized cubic form, with space group $Pm3\bar{m}$ (no. 221). The unit cell of this structure contains one unit formula (Z = 1), with the atomic positions defined by their Wyckoff sites: Ag: 1a (0, 0, 0), X (X = Ca, Sr, Ba): 1b (1/2, 1/2, 1/2), and Br: 3c (1/2, 1/2, 0). The predicted unit cell parameters for AgCaBr3, AgSrBr3, and AgBaBr3 are 5.4815 Å, 5.7490 Å, and 6.1310 Å, respectively. Their expected bandgap energies are 0.73 eV for AgCaBr3 and AgSrBr3, and 0.64 eV for AgBaBr3 [34]. As of now, the $AgXBr_3$ compounds, with X representing Ca, Sr, or Ba, have neither been synthesized nor subjected to experimental study. Building on previous research, our study aims to explore the structural, electronic and optical properties of these three lead-free halide perovskites ($AgXBr_3$, X = Ca, Sr, Ba) as promising eco-friendly materials. To achieve a comprehensive understanding of their properties, we utilized the full-potential linearized augmented plane wave (FP-LAPW) method, implemented in the WIEN2K code [36], along with the recently developed Tran-Blaha modified Becke-Johnson (TB-mBJ) exchange-correlation potential [37] for better describing the electronic structure. This advanced computational technique enables us to provide a detailed analysis of these materials' properties, paving the way for future experimental studies and eventual interesting applications.

his Memory is divided into three main chapters:

- the first provides an overview of ab-initio calculations and discusses single particle self consistent field methods, namely Hartree and Hartree-Fock, as approximations of the multi-body Schrödinger equation. The Hohenberg-Kohn-Sham formulation of the functional theory of density is also introduced. The second chapter will concentrate on the computational tools used in this study, namely the pseudopotential plane-wave (PP PW) method with the GGA-PBEsol and HSE06 functionals for treating exchange correlation effects, as implemented in the CASTEP code, and the full-potential linearized/augmented plane wave plus local orbitals (FP-L/APW + lo) method with both the GGA-PBEsol and Tran-Blaha modified Becke-Johnson (TB-mBJ) potential, as implemented in the WIEN2k package.

- the chapter Three The results of the calculations, which determine the properties of these three lead-free halide perovskites (AgXBr3, X = Ca, Sr, Ba) as promising eco-friendly materials, are presented.

- Finally, a general conclusion is provided regarding this work.

References

[1] U-G Jong, C-J Yu, Y-H Kye, Y-G Choe, W Hao, and S Li Inorg. Chem. 58 4134 (2019).

[2] J-H Lee, Z Deng, N C Bristowe, P D Bristowe, and A K Cheetham J. Mater. Chem. C 6 12252 (2018).

[3] A Kojima, K Teshima, Y Shirai, and T Miyasaka J. Am. Chem. Soc. 131 6050 (2009).

[4] H-S Kim, C-R Lee, J-H Im, K-B Lee, T Moehl, A Marchioro, S-J Moon, R Humphry Baker, J-H Yum, and J E Moser Sci. Rep. 2 591 (2012).

[5] J Tong, Z Song, D H Kim, X Chen, C Chen, A F Palmstrom, P F Ndione, M O Reese, S P Dunfield, O G Reid, J Liu, F Zhang, S P Harvey, Z Li, S T Christensen, G Teeter, D Zhao, M M Al-Jassim, M F A M Van Hest, et al. Science 364 475 (2019).

[6] Md Z Rahaman and M A Islam J. Supercond. Nov. Magn. 34 1133 (2021).

[7] T Yi, W Chen, L Cheng, R D Bayliss, F Lin, M R Plews, D Nordlund, M M Doeff, K A Persson, and J Cabana Chem. Mater. 29 1561 (2017).

[8] N S Arul and V D Nithya (eds) Revolution of Perovskite: Synthesis, Properties and Applications (Singapore : Springer Singapore) (2020).

[9] G H Haertling J. Am. Ceram. Soc. 82 797 (1999).

[10] N Setter and E L Colla (eds) Ferroelectric Ceramics: Tutorial reviews, theory, processing, and applications (Basel : Birkhäuser Basel) (1993).

[11] A Bedjaoui, D Allali, M Radjai, A Bouhemadou, S S Essaoud, S Bin-Omran, R Khenata, and Y Al-Douri Solid State Commun. 387 115532 (2024).

[12] L E Cross and R E Newnham Ceram. Civiliz. 3 289 (1987).

[13] H Jaffe J. Am. Ceram. Soc. 41 494 (1958).

[14] F J Loureiro, N Nasani, G S Reddy, N R Munirathnam, and D P Fagg J. Power Sources 438 226991 (2019).

[15] A S Bhalla, R Guo, and R Roy Mater. Res. Innov. 4 3 (2000).

[16] P Gao, M Grätzel, and M K Nazeeruddin Energy Environ. Sci. 7 2448 (2014).

[17] M A Riza, M A Ibrahim, U C Ahamefula, M A M Teridi, N A Ludin, S Sepeai, and K Sopian Sol. Energy 137 371 (2016).

[18] M Liu, M B Johnston, and H J Snaith Nature 501 395 (2013).

[19] I Chung, B Lee, J He, R P Chang, and M G Kanatzidis Nature 485 486 (2012).

[20] G Natta Rend Accad Naz Lincei 5 1003 (1927).

[21] C P Brock Acta Crystallogr. Sect. A 64 C167 (2008).

[22] Y Zhao and K Zhu Chem. Soc. Rev. 45 655 (2016).

[23] N Sarukura, H Murakami, E Estacio, S Ono, R El Ouenzerfi, M Cadatal, T Nishimatsu, N Terakubo, H Mizuseki, and Y Kawazoe Opt. Mater. 30 15 (2007).

[24] F Zhang, Y Mao, T-J Park, and S S Wong Adv. Funct. Mater. 18 103 (2008).

[25] D Babel Structural chemistry of octahedral fluorocomplexes of the transition elements (eds) C K Jørgensen, J B Neilands, R S Nyholm, D Reinen, and R J P Williams, (Berlin, Heidelberg : Springer Berlin Heidelberg) p 1 (1967).

[26] J Lu, S-C Chen, and Q Zheng ACS Appl. Energy Mater. 1 5872 (2018).

[27] S Cheng, Q Chang, Z Wang, L Xiao, E E M Chia, and H Sun Adv. Opt. Mater. 9 2100564 (2021).

[28] N L Allan, M J Dayer, D T Kulp, and W C Mackrodt J. Mater. Chem. 1 1035 (1991).

[29] P Hagenmuller Inorganic solid fluorides: chemistry and physics (Elsevier) (2012).

[30] J W Fergus Sens. Actuators B Chem. 42 119 (1997).

[31] I J Videau and I Portier Inorg. Solid Fluorides Chem. Phys. 309 (1985).

[32] S S Essaoud, S M Al Azar, A A Mousa, and R S Masharfe Phys. Scr. 98 035820 (2023).

[33] S G Motti, D Meggiolaro, S Martani, R Sorrentino, A J Barker, F De Angelis, and A Petrozza Adv. Mater. 31 1901183 (2019).

[34] J I Gómez-Peralta and X Bokhimi Mater. Chem. Phys. 267 124710 (2021).

[35] J I Gómez–Peralta and X Bokhimi J. Solid State Chem. 285 121253 (2020).

[36] P Blaha, K Schwarz, F Tran, R Laskowski, G K Madsen, and L D Marks J. Chem. Phys. 152 074101 (2020).

[37] F Tran and P Blaha Phys. Rev. Lett. 102 226401 (2009).

CHAPTER I

THEORY OF DENSITY FUNCTIONAL

I. Theory of Density Functional

I.1 Introduction

A solid consists of a collection of positively charged particles (the nuclei) and negatively charged particles (the electrons), which interact through electromagnetic forces. The physical and chemical properties of solids largely depend on the motion of these particles. This motion is governed by the laws of quantum mechanics, and a complete understanding of a quantum system requires the calculation of the wave function, which is achieved by solving the Schrödinger equation

$$\hat{H}\psi = E\psi \tag{I.1}$$

The symbols, and represent, respectively, the Hamiltonian operator, the total energy, and the complete wave function of the system. The exact form of the Hamiltonian in a crystal (within the non-relativistic framework) arises from the effect of electrostatic interaction forces, which can be either attractive or repulsive depending on the charges of the particles (such as electrons and ions).

$$\hat{H} = \hat{T}_n + \hat{V}_{nn} + \hat{V}_{ne} + \hat{V}_{ee} + \hat{T}_e \tag{I.2}$$

$\hat{T}_n$ represents the kinetic energy of the nuclei, $\hat{V}_{nn}$ The potential energy resulting from the interaction between atomic nucleus, $\hat{V}_{ne}$ The potential energy of the attractive interaction between the nucleus and the electrons, $\hat{V}_{ee}$ The potential energy of electrostatic repulsion between electrons, along with the kinetic energy of the electrons.

For a system with N nuclei, the problem to be addressed is a problem with (N+1)Z particles

In the electromagnetic interaction, this implies the presence of 3(N+1)Z variables (in the case where the atoms are identical). Since there are about 5×10^{22} atoms in 1 cm³, by setting Z = 14, the number of variables will be equal to 2×10^{24} [1] . The complexity of this problem would be too great to be solved without resorting to additional simplifications.

The three main levels of simplification are generally as follows:

1. The Born-Oppenheimer approximation (first level of approximation).
2. The Hartree-Fock approximation or the formalism of density functional theory (second level of approximation).
3. The approximations inherent in solving the equations (third level of approximation).

I.2 Level 1: Born-Oppenheimer Approximation

Key Concepts: Treating nuclei as fixed in space...

The Born-Oppenheimer approximation [2] is based on the fact that the mass of the nucleus is about 10^3 to 10^4 times greater than that of the electron, giving it significantly higher inertia. As a result, the nucleus moves much more slowly than the electron. Given this large difference in speed, it is reasonable to assume that the nuclei remain stationary when analyzing the instantaneous motion of the electrons. By adopting this assumption, equation (I.2) can be simplified: the kinetic energy of the nuclei is neglected, and the interaction energy between nuclei becomes constant. This constant can be taken as the reference point for energy (i.e., we set $\hat{T}_n = 0$ and $\hat{V}_{nn} = 0$).Accordingly, the Hamiltonian of the system simplifies to:

$$\hat{H} = \hat{V}_{ne} + \hat{V}_{ee} + \hat{T}_e \qquad \text{(I.3)}$$

Although the model is now simpler than the original formulation, solving it remains challenging due to the complex interactions between a large number of electrons ($\hat{V}_{ee}$). Therefore, it becomes necessary to introduce additional approximations to make the problem more manageable.

I.3 Level 2

I.3.1 Hartree Approximation (Free Electron)

Key Concepts: Free electrons, Hartree product, self-consistent solution...

The Hartree approximation, first introduced in 1928, represents the earliest attempt to find an approximate solution to equation (I.3) [3] . The central idea is that each electron moves in an average electrostatic field created by all other electrons, rather than accounting for individual electron-electron interactions. This approximation simplifies the problem of interacting N electrons by representing it as a single-electron system. The Hartree approximation involves finding the Eigen functions in an approximate form as follows:

$$\Psi_{\text{approchée}} = \Psi_1(\vec{r}_1)\ \Psi_2(\vec{r}_2)\ \ldots\ldots\ldots\ldots\ \Psi_N(\vec{r}_N) \qquad \text{(I.4)}$$

This approximation is based on the assumption of free electrons, meaning spin is ignored. This has two important consequences:

-The total Coulomb repulsion $\hat{V}_{ee}$ of the electronic system is estimated to be greater than its actual value.

-The Pauli exclusion principle is not taken into account.

I.3.2 Hartree-Fock Approximation Method

Concepts: consideration of spin, exchange, variational principle...

An approximation known as the Hartree-Fock method was developed in the 1930s [4] , introduced to account for the spin of electrons in solving the Schrödinger equation. The wave function ψ is expressed using a Slater determinant. The exchange energy is treated exactly, while the correlation energy is only included in more advanced versions.

I.3.3 Density Functional Theory

Key concepts: density distribution, valence electrons, functional, exchange-correlation functional, ...

Density Functional Theory (DFT) is a method for calculating the electronic structure in which the electronic density $\rho(\vec{r})$ takes the central role instead of the many-body wave function, as is the case in the Hartree-Fock method. The fundamental principle of this theory is that all properties of an interacting many-particle system can be considered as a functional of the ground state density $\rho_0(\vec{r})$. Additionally, the exchange energy and correlation energy are both introduced in the calculation in an approximate manner.

In fact, this idea is not new; it first emerged in the works of Thomas [5] and Fermi [6] in the late 1920s. However, it wasn't until the mid-1960s that the contributions of Hohenberg and Kohn [7] on the one hand, and Kohn and Sham [8] on the other, provided the theoretical framework that underlies the DFT used today.

I.3.3.1. Hohenberg-Kohn theorems

-Theorem 1

Density as the fundamental variable: The total energy of the ground state E is a unique functional of the particle density $\rho(\vec{r})$ for a given external potential $V_{ext}(\vec{r})$. Hohenberg and Kohn showed [7] that there is a one-to-one correspondence between the external potential $V_{ext}(\vec{r})$ and the electronic density $\rho(\vec{r})$, allowing the former to be represented as a functional of the ground state of the latter. Consequently, the total energy of the system in the ground state is also a unique, universal functional of the electronic density, as shown in the following equation:

$$E = E[\rho(\vec{r})] \tag{I.5}$$

This theorem is the foundation of Density Functional Theory and explains the name given to it. This differs from the Hartree-Fock method, where the total energy of the system is a functional of the wave function. One immediate consequence of this theorem is that the electronic density uniquely determines the Hamiltonian operator of the system. Therefore, by knowing the

electronic density, the Hamiltonian operator can be determined, and through this Hamiltonian, the various properties of the material can be calculated.

-Theorem 2

The variational principle: The functional of the total energy of any many-particle system has a minimum that corresponds to the ground state and the particle density of the ground state.

Hohenberg and Kohn demonstrated that the total energy of any quantum system of electrons reaches its minimum only when the electronic density $\rho(\vec{r})$ exactly corresponds to the ground state density $\rho_0(\vec{r})$, for a given external potential $V_{ext}(\vec{r})$ and a fixed number of electrons N.

$$E(\rho_0) = minE(\rho) \tag{I.6}$$

The total energy functional in the ground state can be expressed as follows:

$$E\left[\rho(\vec{r})\right] = F\left[\rho(\vec{r})\right] + \int \hat{V}_{ext}(\vec{r})\rho(\vec{r})d^3r \tag{I.7}$$

Where $V_{ext}(\vec{r})$ denotes the external potential acting on the particles, and $F\left[\rho(\vec{r})\right]$ represents the universal functional formulated by Hohenberg and Kohn, defined as follows:

$$F\left[\rho(\vec{r})\right] = \left\langle \Psi | \hat{T} + \hat{V} | \Psi \right\rangle \tag{I.8}$$

Knowing this functional allows us to calculate the total energy and charge density of the ground state for a given external potential, using the variational principle. However, the Hohenberg and Kohn theorem provides no direct information about the exact form of the functional $F\left[\rho(\vec{r})\right]$.

I.3.3.2. Kohn-Sham Approach

Following the development of quantum mechanics, Thomas and Fermi attempted to express the total energy as a function of the electronic density [5,6]. However, the main issue with their approach was the representation of the kinetic energy in the absence of orbitals, which did not allow them to achieve satisfactory accuracy. After about four decades of efforts, the Kohn-Sham approach eventually [8] became the dominant method because it leaves only one term of the total energy undetermined, and it is the smallest one: the exchange-correlation term. The core idea of the Kohn-Sham theorem is to replace a real interacting system with a fictitious non-interacting system. This approach achieves an exact correspondence between the electronic density, the ground-state energy of a system consisting of non-interacting fermions placed in an effective potential, and the real system of interacting electrons subjected to the actual potential. As a result, the electronic density and energy of the real system are preserved within this fictitious system (see Figure I.1).

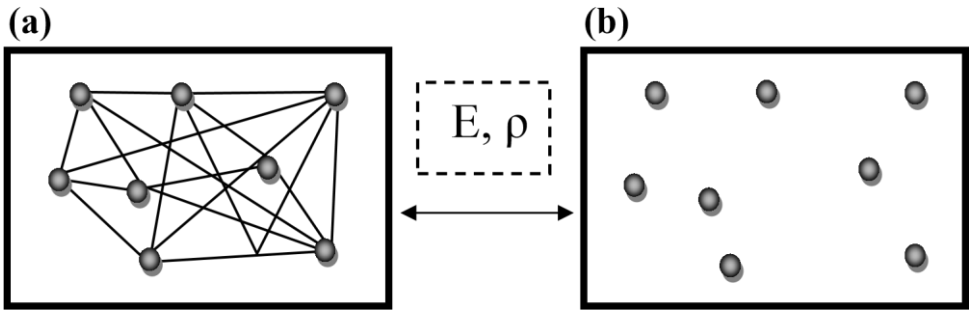

Figure I.1: (a) Real system consisting of multiple interacting electrons; (b) Fictitious system of independent fermions with the same energy and electronic density as the real system.

The Hohenberg and Kohn theorems also apply to this fictitious system. The universal functional of Hohenberg and Kohn $F[\rho(\vec{r})]$ for the interacting system can be expressed by the following equation:

$$F[\rho(\vec{r})] = T_0[\rho(\vec{r})] + E_H[\rho(\vec{r})] + E_{xc}[\rho(\vec{r})] + V_{ext}[\rho(\vec{r})] \quad (I.9)$$

where:

$T_0[\rho(\vec{r})]$: represents the kinetic energy of a system of non-interacting electrons,

$E_H[\rho(\vec{r})]$: represents the Hartree term, i.e., the classical Coulomb interaction between electrons described through their charge density,

$E_{xc}[\rho(\vec{r})]$: is an additional functional used to describe the exchange-correlation energy arising from electron-electron interactions,

$V_{ext}[\rho(\vec{r})]$: includes the Coulomb interaction between electrons and nuclei, as well as the interaction between the nuclei themselves.

The Hartree term and the kinetic energy play a key role in describing the states of free electrons, as they are among the most significant components in handling electron interactions. The difference between the actual kinetic energy and that of non-interacting electrons, as well as the difference between the real interaction energy and the Hartree energy, are accounted for in the exchange-correlation energy $E_{xc}[\rho(\vec{r})]$. The Schrödinger equation to be solved within the Kohn-Sham approach is written as follows:

$$\left[-\frac{\hbar^2}{2m_e}\vec{\nabla}_i^2 + \hat{V}_{eff}(\vec{r})\right]\left|\Phi_i(\vec{r})\right\rangle = \varepsilon_i\left|\Phi_i(\vec{r})\right\rangle \qquad (i=1,\ldots,N) \quad (I.10)$$

The effective potential is expressed in the following form:

$$V_{eff} = \hat{V}_{ex} + \int \frac{\rho(\vec{r}')}{|\vec{r} - \vec{r}'|} dr' + \hat{V}_{xc} \quad \text{(I.11)}$$

The exchange-correlation potential is given by the functional derivative of the following:

$$\hat{V}_{xc} = \frac{\partial E_{xc}[\rho(\vec{r})]}{\partial \rho(\vec{r})} \quad \text{(I.12)}$$

The density is given by the sum over all occupied orbitals:

$$\rho(\vec{r}) = \sum_{i=1}^{N} | \Phi_i(\vec{r}) |^2 \quad \text{(I.13)}$$

Equations (I.10)are the Kohn-Sham equations and are solved in a self-consistent manner, starting from an initial density and a potential $\hat{V}_{eff}(\vec{r})$.

A solution is obtained in which equation (I.10) is solved, and a new electronic density is then determined. From this new density, an updated effective potential can be calculated. This process is repeated self-consistently until convergence is reached, that is, when the new electronic density becomes equal to or very close to the previous one, according to the chosen convergence criterion.

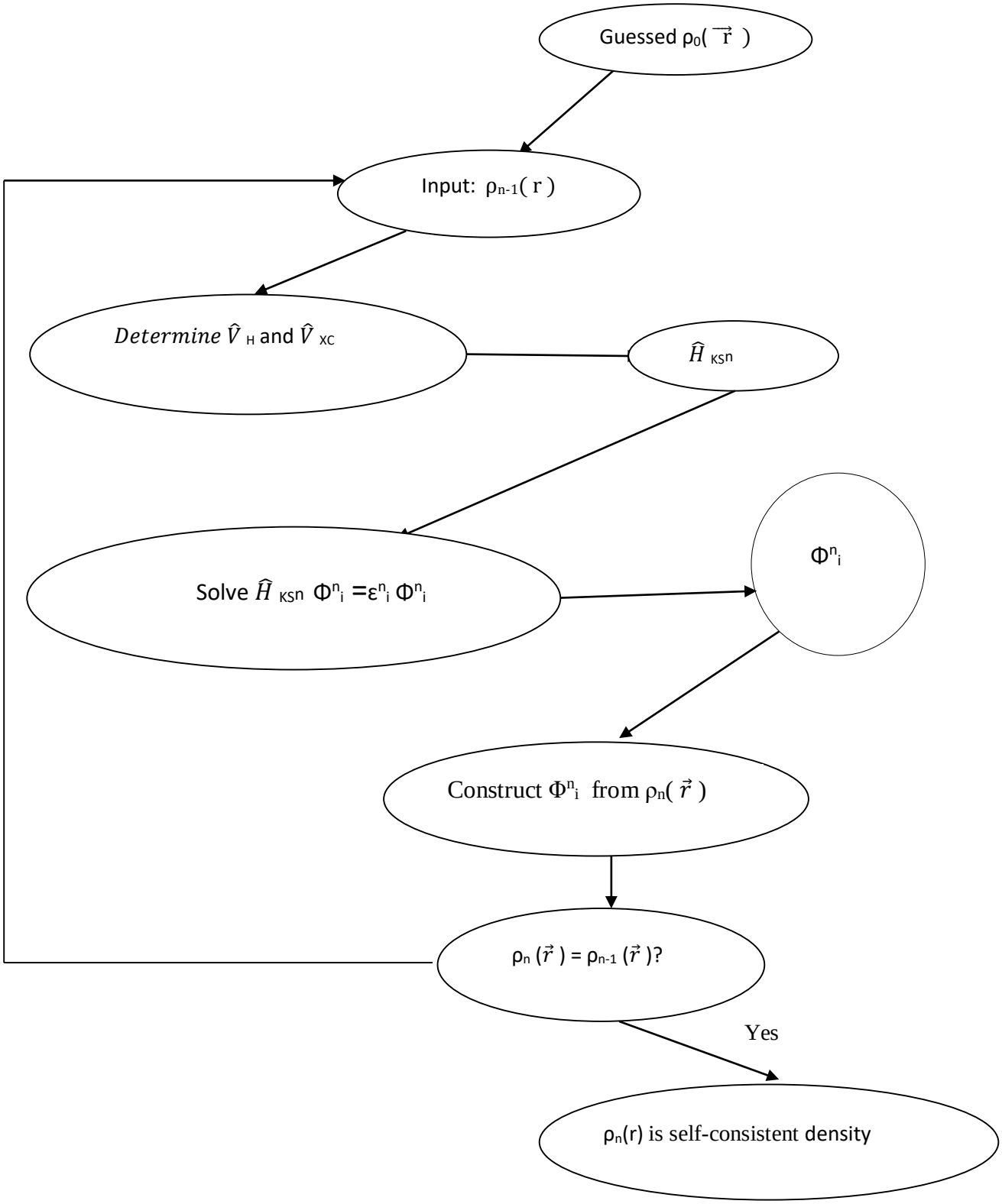

Figure I.2: Flowchart for the iterative solution of the Kohn-Sham equations

I.3.3.3 Approximations of the exchange-correlation functional

Many approximations have been developed for E_{XC}, since the exact expression for this functional has not yet been found. In fact, this functional encapsulates all the challenges of many-body problems. The form of the exchange-correlation functional determines the accuracy of calculations in DFT, yet there is no strict rule regarding the suitability of an exchange-correlation functional for a given chemical structure.

The effects resulting from interactions between electrons are divided into three categories:

Exchange effect

This effect, also known as Fermi correlation**,** arises from the requirement that the total wave function of electrons be antisymmetric when two particles are exchanged. This means that two electrons with the same spin orientation cannot occupy the same point in space the probability of them being found together at the same location is zero. This behavior is directly related to the Pauli exclusion principle and does not involve the electrostatic repulsion between electrons**.** It results purely from the quantum nature of electrons as fermions**.** This effect is naturally accounted for in the Hartree-Fock approximation[4]**,** due to the way the wave function is constructed using a Slater determinant**,** which enforces the required antisymmetry.

Coulomb correlation.

It is due to the electric charge of the electron and is related to the repulsion between electrons according to the relation $\frac{1}{|\vec{r}-\vec{r}'|}$. Unlike the exchange effect, it is independent of the spin.

This effect is neglected in the Hartree-Fock theory.

Self-interaction correction

The third effect arises from the fact that electronic wave functions are based on the assumption of independent particles. This is known as the self-interaction correction, which aims to ensure the correct counting of electron pairs. The exchange-correlation functional must also take into account the difference in kinetic energy between the non-interacting reference system and the real system. Therefore, the calculation of the exchange-correlation energy and potential relies on a set of approximations.

I.3.3.3.1 Local Density Approximation

In the Local Density Approximation (LDA), it is assumed that the electronic density can be treated locally as a uniform electron gas. This amounts to making the following two assumptions:

- The exchange-correlation effects are primarily dominated by the density at the point
- The density $\rho(\mathrm{r})$ is a function that varies slowly with respect to $\vec{r}$.

This approximation assumes that the contribution of $E_{xc}\left[\rho(\vec{\mathrm{r}})\right]$ to the total energy of the system can be gradually accumulated from each region of the inhomogeneous gas, as if each region behaves like a locally homogeneous gas. According to the LDA approximation, the exchange-correlation energy is written as follows:

$$E_{xc}^{LDA}\left[\rho(\vec{\mathrm{r}})\right]=\int\rho(\vec{\mathrm{r}})\grave{o}_{xc}^{LDA}\left[\rho(\vec{\mathrm{r}})\right]d^{3}\mathrm{r} \tag{I.14}$$

$\grave{o}_{xc}^{LDA}\left[\rho(\vec{r})\right]$ represents the exchange-correlation energy per electron in an electron gas assumed to have a uniform distribution. From $\grave{o}_{xc}^{LDA}\left[\rho(\vec{r})\right]$, the exchange-correlation potential $V_{xc}^{LDA}(\vec{r})$ can be derived variationally according to the following equation:

$$V_{xc}^{LDA}(\vec{\mathrm{r}})=\frac{\delta(\rho(\vec{\mathrm{r}})\grave{o}_{xc}^{LDA}\left[\rho(\vec{\mathrm{r}})\right]}{\delta\rho(\vec{\mathrm{r}})} \tag{I.15}$$

In magnetic systems, the electron spin introduces an additional degree of freedom, requiring the extension of the Local Density Approximation (LDA) to the Local Spin Density Approximation (LSDA), where the exchange-correlation energy is a functional of the densities of the spin-up and spin-down electrons.

$$E_{xc}^{LSDA}\left[\rho_{\uparrow},\rho_{\downarrow}\right]=\int\rho(\vec{r})\grave{o}_{xc}\left[\rho_{\uparrow}(\vec{\mathrm{r}}),\rho_{\downarrow}(\vec{\mathrm{r}})\right]d^{3}\mathrm{r} \tag{I.16}$$

The Local Density Approximation (LDA) assumes that the functional BBB is purely local. This energy is divided into two terms:

$$\grave{o}_{xc}^{LDA}\left[\rho(\vec{\mathrm{r}})\right]=\grave{o}_{x}\left[\rho(\vec{\mathrm{r}})\right]+\grave{o}_{c}\left[\rho(\vec{\mathrm{r}})\right] \tag{I.17}$$

Here, $\grave{o}_{x}\left[\rho(\vec{r})\right]$ refers to the exchange energy, while $\grave{o}_{c}\left[\rho(\vec{r})\right]$ represents the correlation energy. The exchange energy for a uniform electron gas is expressed using the Dirac-Fermi formula in terms of the density $\rho^{1/3}$, and is defined in atomic units as follows:

$$\grave{o}_{x}^{LDA}[\rho(\mathrm{r})]=-0.4581/\mathrm{r}_{s} \tag{I.18}$$

With $\rho=(4\pi\mathrm{r}_{s}^{3}/3)^{-1}$

For the first time, the term "correlation" was estimated by Wigner through:

$$\grave{o}_x^{LDA}[\rho(\vec{r})]=\frac{0.44}{r_s+7.8} \qquad (I.19)$$

The correlation energy of a free electron gas was modeled by Ceperley and Alder [9], and this modeling was presented by Perdew and Zunger [10] as follows:

$$\grave{o}_c[\rho(\vec{r})]=\frac{-0.1423}{1+1.0529\sqrt{r_s}+0.3334r_s} \qquad r_s>1 \qquad (I.20)$$

$$\grave{o}_c[\rho(\vec{r})]=-0.048+0.0311\ln r_s-0.0116r_s+0.002r_s\ln r_s \qquad r_s<1 \qquad (I.21)$$

There are other parameterizations for the correlation energy of a homogeneous electron gas, such as those by Kohn and Sham [7], Hedin and Lundqvist [11], and Perdew and Wang [12]. Since the Local Density Approximation (LDA) is defined based on a homogeneous electron gas, it would be expected to provide good results only for systems with slowly varying electronic density. However, the applicability of LDA extends beyond this, and it has produced good results even for systems with inhomogeneous density. Experimental results have shown that LDA performs better than the Hartree-Fock approximation in many cases [13] .

Typically, calculations using the Local Density Approximation (LDA) result in excessively high binding energies. This leads to shorter bond lengths, smaller lattice parameters, and larger incompressibility moduli than expected.

I.3.3.3.2 The Generalized Gradient Approximation (GGA)

The first step taken to improve the treatment of exchange-correlation energy is to make the energy functional $E_{xc}\left[\rho(\vec{r})\right]$ dependent not only on the electronic density but also on its gradient $\left|\vec{\nabla}\rho(\vec{r})\right|$. With this modification, the functional $\Phi_m(\vec{r})$ accounts for the non-uniform nature of the electron gas.

On the other hand, GGA functionals cannot be classified as non-local methods because they depend solely on the density (and its first derivatives) at a specific point, rather than on a volume of space, as is the case with exchange energy in the Hartree-Fock method. The non-local property is only realized by other categories of functionals.

In the GGA formalism, the contribution of $E_{xc}\left[\rho(\vec{r})\right]$ to the total energy of the system can be accumulated from each region of the inhomogeneous electron gas, as if it were locally inhomogeneous. This definition of the GGA functional implies that it takes the following

form:

$$E_{xc}^{GGA}\left[\rho(\vec{r})\right]=\int\rho(\vec{r})\dot{o}_{xc}\left[\rho(\vec{r}),\left|\nabla\rho(\vec{r})\right|\right]d^3r \quad (I.22)$$

Where $\dot{o}_{xc}\left[\rho(\vec{r}),\left|\vec{\nabla}\rho(\vec{r})\right|\right]$ denotes the exchange-correlation energy per electron in a system of interacting electrons with a non-uniform density.

The adoption of GGA-type functionals [14,15] greatly enhanced the accuracy of computational results compared to those obtained using the LDA approach, especially in calculating molecular binding energies. This improvement was a key factor in the widespread use of Density Functional Theory (DFT) by chemists during the 1990s.

On the other hand, due to its local nature, the GGA functional fails to accurately describe systems involving Van der Waals interactions, as these interactions rely on long-range correlations.

There are several different parametrizations of the GGA functional, notably those developed by Perdew and collaborators [16,17] in 1991 and 1996. The most widely used versions are those by Perdew and Wang[18] , as well as Perdew's own formulation [19].

I.3.3.3.3 Additional improvements

Exchange, as obtained within the LSDA framework, is considered locally, i.e., at the site where it is calculated. This can be a significant limitation, as this exchange actually encompasses all sites in the lattice as described in the Hartree-Fock approximation. For this reason, new approaches aim to develop hybrid functionals that involve exchange in the Hartree-Fock approximation, such as exact exchange**.**

I.4 Level 3: solving the Schrödinger equation

The solution of the Kohn-Sham equation is not done directly, which forces us to describe it in a finite basis of functions ϕ as follows:

$$\phi_m=\sum_{p=1}^{P}C_p^m\phi_p^b \quad (I.23)$$

The solution of the Schrödinger equation involves determining the coefficients C^m_p needed to express $\phi_m(r)$ in a basis of functions ϕ^b_p. This process constitutes the third level of approximation used to obtain a practically usable treatment of the foundations of these theories. In fact, wave functions belong to a function space that has an infinite dimension P. Therefore, P in equation (I.23) is strictly infinite. As a result, a finite basis can never describe $\phi_m(r)$ exactly. However, the goal of quantum chemistry calculations is to find the basis that allows for the

closest possible approximation of $\phi_m(r)$. After choosing a basis and thus a finite value for P, the Schrödinger equation (1.10) can be transformed into the secular form.

$$\begin{bmatrix} \cdots & \cdots & \cdots \\ \vdots & \left\langle \phi_i^b | \hat{H}_{sp} | \phi_j^b \right\rangle > -\varepsilon_m \left\langle \phi_i^b | \phi_j^b \right\rangle & \vdots \\ \cdots & \cdots & \cdots \end{bmatrix} \begin{bmatrix} c_1^m \\ \vdots \\ c_p^m \end{bmatrix} = \begin{bmatrix} 0 \\ \vdots \\ 0 \end{bmatrix} \tag{I.24}$$

Where the matrix elements of the single-particle Hamiltonian and the overlap matrix elements can be identified.

$$\left(H_{ij} - \varepsilon_m S_{ij}\right) C_p^m = 0 \tag{I .25}$$

where $H_{ij} = \langle \phi_i^b | \hat{H} | \phi_j^b \rangle$ and $S_{ij} = \langle \phi_i^b | \phi_j^b \rangle$ They represent, respectively, the Hamiltonian and overlap matrices.

For a solid, these equations must be solved for each k-point in the irreducible Brillouin zone. This system of secular equations is linear with respect to energy. It represents an eigenvalue problem for S_m and Eigen functions for $\Phi_i^k(\vec{r})$, which is well-known within the framework of Hartree-Fock theory, and is typically solved using standard numerical methods.

The criteria for evaluating a basis set are its efficiency, simplicity, and accuracy. These three main characteristics are reflected in:

-The number of basis functions required to achieve convergence.

-Whether the basis favors certain regions of the species more than others (e.g., being more flexible near the nuclei).

-The difficulty in calculating matrix elements for different operators.

-The difficulty of improving or modifying the basis by arbitrarily adding functions of the same type.

References

[1] P. Kiréev, *la physique des semi-conducteurs,* Edition Mir, Moscou (1979).

[2] M. Born, J.R. Oppenheimer, Zur quantentheorie der Molekeln, Ann. Phys. 84 (1927) 45.

[3] D.R. Hartree, Proc. Combridge Philos. Soc. 24 (1928) 89.

[4] V. Fock, Z. Phys. 61 (1930) 126; 62 (1930) 795.

[5] L.H. Thomas, Proc. Cambridge Philos. Soc. 23 (1927) 542.

[6] E. Fermi, *Z. Phys*. 48 (1928) 73.

[7] P. Hohenberg, W. Kohn, Phys. Rev. B. 136 (1964) 864.

[8] W. Kohn, L.J. Sham, Phys. Rev. A. 140 (1965) 1133.

[9] D.M. Ceperley, B. J. Alder, Phys. Rev. Lett. B 23 (1980) 5048.

[10] J.P. Perdew, A. Zunger, Phys. Rev. B. 23 (1981) 5048.

[11] L. Hedin, B. Lundqvist, J. Phys. C. 4 (1971) 2064.

[12] J.P. Perdew, Y. Wang, Phys. Rev. B. 45 (1992) 13244.

[13] M.C. Holthausen, W. Koch. *A Chemist's Guide to Density Functional Theory*. Wileyvch, Weinheim (Allemagne). 2000.

[14] K. Burke, J.P. Perdew, M. Ernzerhof, J. Chem. Phys. 109 (1998) 3760.

[15] J.P. Perdew, K. Burke, Y. Wang, Phys. Rev. B. 54 (1996) 16533.

[16] J.P. Perdew , J. A. Chevary, S. H. Vosko, K. A. Jackson, M. R. Pedreson, D.J. Singh, C. Fiolhais, Phys. Rev. B. 43(1992) 6671.

[17] J.P. Perdew, S. Burke, M. Ernzerhof, Phys. Rev. Lett. 77 (1996) 3865.

[18] J.P. Perdew, Y. Wang, Phys. Rev. B. 33(1986) 8800.

[19] J.P. Perdew, *Electronic Structure of Solids*, Academie Verlag, Berlin. 11 (1991).

CHAPTER II

PLANES WAVES AND PSEUDOPOTENTIAL METHOD

II. **Planes Waves and Pseudopotential Method**

II.1. **Introduction**

To solve the Kohn-Sham equations, it is important to choose a basis that is suitable for the characteristics of the studied system. This allows for the expansion of the Kohn-Sham eigenstates and the expression of the different components of the Hamiltonian. When studying crystalline materials, plane waves are considered a suitable choice because the periodic structure of crystals allows us to exploit symmetry to reduce the number of atoms needed in the calculations. However, plane waves exhibit rapid oscillations near the atomic nuclei, which requires a large number of basis functions to accurately represent these regions. This issue can be mitigated using the pseudopotential approximation, where the effects of the nucleus and core electrons are replaced with an effective potential. This significantly reduces the number of required basis functions and thus lowers computational cost. The combination of the plane wave basis with the pseudopotential approximation is known as the pseudopotential plane wave method. In this chapter, we will present the formulation of the Kohn-Sham equations in the plane wave basis, explain the pseudopotential approximation, and then outline a practical procedure for solving these equations.

II.2. **Crystal symmetry and Bloch's theorem**

II.2.1. **Periodic systems**

A crystal is an ordered state of matter characterized by the periodic repetition of atomic nuclei positions in space, which results in the repetition of all physical properties in the same pattern. The crystal can be fully described in real space by a set of non-coplanar primitive basis vectors $\vec{b}_1$, $\vec{b}_2$, $\vec{b}_3$, along with the positions of atoms within the primitive unit cell (PUC).

The lattice vectors are constructed from all possible linear combinations of the primitive vectors, each multiplied by an integer:

$$\vec{R} = n_1\vec{b}_1 + n_2\vec{b}_2 + n_3\vec{b}_3 \qquad \text{(II.1)}$$

Where n_1, n_2, n_3 are integers.

The lattice generated by this type of translational operation is known as a simple Bravais lattice. The parallelepiped defined by the three basis vectors $\vec{b}_1$, $\vec{b}_2$, $\vec{b}_3$ is called the unit cell of the Bravais lattice, or the primitive cell. The volume of this cell is given by:

$$\vec{V} = \vec{b}_1 \times \left(\vec{b}_2 \times \vec{b}_3\right) \qquad \text{(II.2)}$$

There are unlimited possible shapes for the unit cell, but the one that has the highest degree of symmetry and the most geometrically compact form is called the Wigner-Seitz cell.

Since the motion of electrons in a crystal is typically described in both real space and momentum space (or k-space), it is essential to introduce the concept of the reciprocal lattice, which is the geometric counterpart (or inverse) of the real lattice. In the reciprocal lattice, a set of reciprocal basis vectors $\vec{b}^*_1$, $\vec{b}^*_2$, $\vec{b}^*_3$ can be defined based on the original basis vectors $\vec{b}_1$, $\vec{b}_2$,$\vec{b}_3$ of the direct lattice.

These vectors are determined according to the following relation [1]:

$$\vec{b}^*_1 = \frac{2\pi(\vec{b}_2\times\vec{b}_3)}{\vec{b}_1.(\vec{b}_2\times\vec{b}_3)}\,,\ \vec{b}^*_2 = \frac{2\pi(\vec{b}_3\times\vec{b}_1)}{\vec{b}_2.(\vec{b}_3\times\vec{b}_1)}\,,\ \vec{b}^*_3 = \frac{2\pi(\vec{b}_1\times\vec{b}_2)}{\vec{b}_3.(\vec{b}_1\times\vec{b}_2)} \qquad (\text{II.3})$$

The primitive cell in momentum space (reciprocal space) does not necessarily have to be a parallelepiped; instead, one can define the Wigner-Seitz cell of the reciprocal lattice, which is known as the **first Brillouin zone** in reciprocal space. In a perfect crystal, the Hamiltonian H in the Schrödinger equation for a system of particles remains unchanged under any translation operation T(n), since the effective potential shares the same periodicity as the lattice, and the derivative operator is unaffected by translational operations [2].

II.2.2 Bloch's theorem

When solving the Schrödinger equation for a periodic system, the solutions must exhibit a characteristic known as **Bloch's theorem** [3], which states that the Eigen functions can be represented as plane waves modulated by functions that have the same periodicity as the crystal lattice. Using Bloch's theorem, the solutions to the Schrödinger equation in the presence of a periodic potential are given as follows:

$$\psi_{n,k}(r) = \exp(ikr)\, u_{n,k}(r) \qquad (\text{II.4})$$

The function $u_{n,k}(r)$ is a periodic wave function that satisfies $u_{n,k}(r)=u_{n,k}(r+R)$, where R is any vector connecting equivalent points in the Bravais lattice. The vector k lies in reciprocal space and is used to label quantum states; it can always be translated back into the first Brillouin zone. The subscript n denotes the band index, which distinguishes between different Eigen energies $\varepsilon_{n,k}$ corresponding to the same wave vector k. Moreover, the eigenvalues themselves are periodic functions in reciprocal space, i.e.:

$$\varepsilon_{n,k} = \varepsilon_{n,k+K} \qquad (\text{II.5})$$

In other words, Bloch's theorem allows us to reduce the number of electrons considered in the calculations to only those within a single unit cell of the lattice, provided that the system's Hamiltonian is invariant under translational operations.

The periodicity of the function $u_{n,k}(r)$ implies that it can be expanded in terms of a specific set of plane waves that share the same periodicity as the crystal lattice.

$$u_{n,k}(r) = \sum_G \tilde{u}_G \exp(iGr) \quad \text{(II.6)}$$

Where the summation is over all the vectors defined by G:

$$\vec{G} = m_1\vec{b}_1^* + m_2\vec{b}_2^* + m_3\vec{b}_3^* \quad \text{(II.7)}$$

That is m_1, m_2, m_3 are integers, $\vec{b}_1^*$, $\vec{b}_2^*$, $\vec{b}_3^*$are the basis vectors of the reciprocal lattice, and $\tilde{u}_G$ are the expansion coefficients in the series representation.

By combining equations (II.4) and (II.6), it becomes clear that the single-particle wave functions $\psi_{n,k}(r)$, at each point k within the Brillouin zone of a given crystal, can be expressed as a discrete set of plane waves:

$$\psi_{n,k}(r) = \sum_{|G+k|<G_{cut}} c_{nk}(G) \exp[\, i(k+G).r] \quad \text{(II.8)}$$

II.3. **Expression of Kohn-Sham equations in the plane wave basis**

Representing the electron wave functions using plane waves greatly simplifies the formulation of the Kohn-Sham equations in reciprocal space [4,5].

By substituting the electronic wave function, expressed as a sum of plane waves:

$$\left[-\frac{1}{2}\nabla^2 + V_{eff}\right]\psi_i(r) = \varepsilon_i\psi_i(r) \quad \text{(II.9)}$$

into the Kohn-Sham equation:

$$\hat{V}_H(r) = \frac{\delta E_H[\rho(r)]}{\delta\rho(r)} = \int \frac{\rho(r_j)}{|r-r_j|}dr_j \quad \text{(II.10)}$$

and performing the integration over **r**, we obtain a matrix eigenvalue equation.

$$\left[\sum_{G'} \frac{1}{2}|k+G|^2\delta_{GG'} + V_{ext}(G-G') + V_{xc}(G-G') + V_H(G-G')\right] = \varepsilon_i C_{Gnk} \quad \text{(II.11)}$$

In equation (II.11), the kinetic energy term appears in a diagonal form, while the other three terms on the left-hand side represent the Fourier components of the external potential, the exchange-correlation potential, and the Hartree potential, respectively.

II.4. The cut-off energy

Theoretically, an exact representation of the electronic wave function requires an infinite set of plane waves. However, in practice, the functions appearing in equation (II.8) can be simply interpreted as solutions to the Schrödinger equation, representing states with a kinetic energy equal to:

$$E = \frac{h^2}{2m}|k+G| \quad \text{(II.12)}$$

In general, as the value of |G| increases, the kinetic energy of the plane wave also increases, which makes its contribution to the wave function expansion less significant. This is because the expansion coefficients $c_{n,k}(G)$ associated with plane waves of high kinetic energy are negligible compared to those associated with plane waves of lower kinetic energy.

Therefore, the number of reciprocal lattice vectors can be reduced by setting an upper limit for the kinetic energy of the plane waves. This limit is called the cut-off energy, and only plane waves with kinetic energy lower than $\mathbf{E_{cut}}$ are included in the expansion of the Kohn-Sham functions. As a result, the infinite sum is reduced to:

$$\psi_{n,k}(r) = \sum_{|G+k|<G_{cut}} c_{nk}(G) \exp[\, i(k+G).r] \qquad \text{(II.13)}$$

It is evident that the value of $\mathbf{E_{cut}}$ impacts the accuracy of the calculations and is strongly dependent on the elements present in the system being studied. Simple convergence tests should be carefully performed in each case by varying the cut-off energy and determining the energy at which convergence is achieved (i.e., increasing the cut-off energy no longer affects the calculated energy of the system).

II.5. Sampling the Brillouin Zone

To calculate many physical properties, such as the total energy of a crystal, it is necessary to know the Bloch functions at an infinite number of k-points within the Brillouin zone, since each k-point corresponds to a distinct set of eigenvalues of the Kohn-Sham equation. However, in practice, a finite set of k-points is selected for calculations.

Because electronic wave functions vary very little between closely spaced k-points, it is possible to represent the behavior in a region of k-space using the wave function at a single k-point [7]. This removes the need to consider an infinite number of electrons and allows calculations to be performed using a limited number of k-points.

By taking advantage of the crystal's additional symmetries, such as mirror reflections and rotations, the number of required k-points can be further reduced. As a result, wave functions ψ only need to be computed at special k-points within the Brillouin zone, and the integration can be confined to a smaller region. The smallest region that, through symmetry operations, can generate the entire Brillouin zone is called the irreducible Brillouin zone (IBZ).

There are several methods for selecting specific points within the Brillouin zone [8,9,10], but the Monkhorst-Pack method is the most commonly used [1].

This method approximates the integration over the Brillouin zone by a weighted sum over a set of special k-points.

By increasing the density of the k-points within the Brillouin zone, the calculation errors can be significantly reduced.

II.6. Pseudopotential

II.6.1 The frozen core approximation

It is well established in chemistry that core electrons, unlike valence electrons, are strongly bound to the nucleus and do not take part in chemical bonding between atoms [12,13]. When an atom moves from one chemical environment to another, the wave functions of its core electrons remain largely unchanged because they have minimal overlap with the core electron wave functions of neighboring atoms. As a result, core electrons have little influence on the electronic and optical properties of materials [14]. Therefore, it is reasonable to assume that the distribution of core electrons within a solid remains "frozen," just as it is in the isolated atom. Based on this assumption, the potential created by the core electrons can be combined with the Coulomb potential of the nucleus to form what is known as the ionic core potential. This allows us to eliminate the core electrons from the calculations and focus solely on the valence electrons a simplification known as the frozen core approximation [15]. Although this approximation introduces only a minor error, it significantly reduces the computational cost.

II.6.2 Concept of pseudopotentials

Since atomic wave functions are eigenstates of the atomic Hamiltonian, they must be orthogonal to each other. This means that the valence electron wave function must differ significantly from the core electron wave functions, often by exhibiting rapid oscillations and having nodes (points where the wave function equals zero) near the nucleus. However, accurately representing these rapid oscillations using a fixed basis set (like plane waves or Gaussian functions) is very challenging and requires a very large number of basis functions. This makes all-electron calculations extremely computationally demanding. Therefore, it's essential to reduce the size of the basis set in order to make the calculations more feasible.

Since valence electrons are responsible for chemical bonding, it is not necessary to describe their behavior accurately in the region close to the nucleus where the core electrons reside. Therefore, it is appropriate to replace the true potential which includes the effects of the

nucleus and the core electrons with a simplified effective potential known as a pseudopotential, which acts only on the valence electrons.

This substitution allows us to avoid the rapid oscillations that appear in the true wave function near the nucleus by using a smoother pseudo wave function that is easier to represent mathematically.

The pseudopotential must also be transferable across different chemical environments; in other words, a pseudopotential constructed for an isolated atom should ideally work just as well for the same element in a compound or other environment without requiring any modifications. For this reason, the pseudo wave function must match the true valence wave function in the bonding region outside the ionic core, where interaction with other atoms [15] occurs as illustrated in Figure II.1.

It is also important that the pseudopotential be as smooth as possible within the core region [16,17]. as this helps reduce the number of basis functions needed to represent the wave functions, thereby minimizing computational complexity.

The pseudopotential method is used to reduce the number of basis functions needed for calculations involving systems with many atoms, thus lowering the computational cost. Pseudopotentials that require high cut-off energies are referred to as "hard," as they demand more computational resources. On the other hand, pseudopotentials that are more computationally efficient, requiring low cut-off energies, are called "soft."

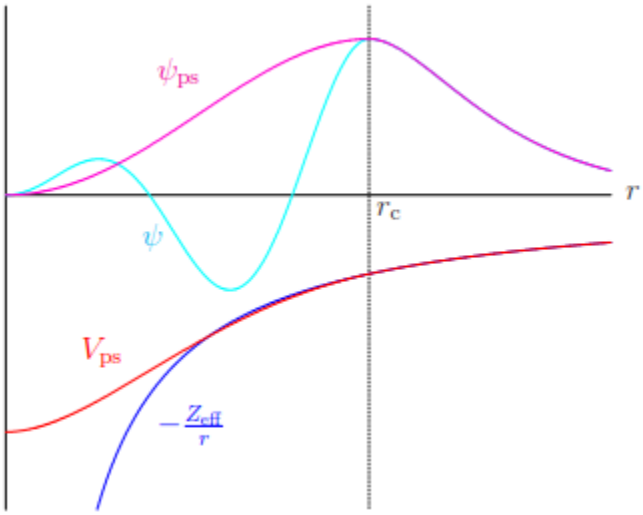

Fig. II.1 A diagram illustrating the relationship between all-electron, approximate (pseudopotential) potentials, and wave functions

II.6.3 Ab initio Pseudopotentials

There is no fixed method for generating a pseudopotential for a specific chemical element; the process allows for considerable flexibility in its construction [18-20].

In the past, empirical pseudopotentials which are not derived from first principles were developed by fitting to experimental data [21,22]. While these pseudopotentials are easy to use, they lack a crucial feature: transferability. They may perform well in specific environments, but are unreliable when applied to different conditions.

Today, many pseudopotentials are developed using non-empirical methods. Those derived from atomic calculations without fitting to experimental data are known as ab initio pseudopotentials. This approach has become a well-established and widely used tool in condensed matter physics, computational chemistry, and materials science.

The use of pseudopotentials began with Fermi's work in the 1930s, aimed at studying high-energy atomic levels [23]. However, the most refined and systematic formulation of a non-empirical pseudopotential was introduced by Phillips and Kleinman [24,25], who developed a rigorous theoretical framework for the pseudopotential method.

II.6.3.1 Method of Philips and Kleinman

To explain the pseudopotential concept proposed by Phillips and Kleinman, we distinguish between the states of the valence electrons $|\psi_v\rangle$ and the states of the core electrons $|\psi_c\rangle$ in a given Hamiltonian (for example, the Fock operator in Hartree-Fock theory or the Kohn-Sham operator in density functional theory).

The wave functions of the core electrons are defined as follows:

$$\hat{H}|\psi_c\rangle = \varepsilon_c|\psi_c\rangle \qquad (c = 1, N_c) \tag{II.14}$$

The wave functions for the valence electrons in this same Hamiltonian are given by:

$$\hat{H}|\psi_v\rangle = \varepsilon_v|\psi_v\rangle \qquad (v = 1, N_v) \tag{II.15}$$

The valence electron wave function $|\psi_v\rangle$ has a number of radial nodes because it must be orthogonal to the core orbitals. Phillips and Kleinman demonstrated that a smooth valence wave function $|\hat{\psi_v}\rangle$, which is not orthogonal to the core state ($\langle\hat{\psi_v}|\psi_c\rangle \neq 0$), can be constructed by combining the core wave functions $|\psi_c\rangle$ with the real valence wave function $|\psi_v\rangle$ in the following manner:

$$|\hat{\psi}_v\rangle = |\psi_v\rangle + \sum_{c=1}^{N_c} b_c|\psi_c\rangle \tag{II.16}$$

The coefficients bc are currently unknown constants, and $|\psi_c\rangle$ represents the core wave functions. These constants can be determined by making use of the fact that the core wave functions are orthonormal, and that $|\psi_v\rangle$ is orthogonal to the core states. By multiplying Equation. (III.16) by one of the core wave functions, such as $|\psi_{c0}\rangle$, and integrating, we obtain:

$$\langle\psi_{c0}|\hat{\psi}_v\rangle = \langle\psi_{c0}|\psi_v\rangle + \sum_c b_c \langle\psi_{c0}|\psi_c\rangle \quad \text{(II.17)}$$

Where

$$\langle\psi_{c0}|\hat{\psi}_v\rangle = b_{c0} \quad \text{(II.18)}$$

Given that $|\psi_v\rangle$ and $|\psi_c\rangle$ are solutions of the Schrödinger equation with eigenvalues ε_v and ε_c respectively, one can easily derive the following equation for the modified wave function $|\hat{\psi_v}\rangle$:

$$\left[\hat{H} + \sum_{c=1}^{N_c}(\varepsilon_v - \varepsilon_c)|\psi_c\rangle\langle\psi_c|\right]|\hat{\psi}_v\rangle = \varepsilon_v|\hat{\psi}_v\rangle \quad \text{(II.19)}$$

$$\left[\hat{T} + \hat{V} + \sum_{c=1}^{N_c}(\varepsilon_v - \varepsilon_c)|\psi_c\rangle\langle\psi_c|\right]|\hat{\psi}_v\rangle = \varepsilon_v|\hat{\psi}_v\rangle \quad \text{(II.20)}$$

The previous result indicates that a pseudo-Hamiltonian can be formulated:

$$\hat{H}_{PS} = \hat{T} + \hat{V}_{ps} \quad \text{(II.21)}$$

With a pseudopotential

$$V_{PS} = V + \sum_{c=1}^{N_c}(\varepsilon_v - \varepsilon_c)|\psi_c\rangle\langle\psi_c| \quad \text{(II.22)}$$

So,

$$\hat{H}_{Ps}|\hat{\psi}_v\rangle = \varepsilon_v|\hat{\psi}_v\rangle \quad \text{(II.23)}$$

This equation shows that the states $|\hat{\psi_v}\rangle$ satisfy a Schrödinger-like equation with an additional contribution, $\hat{V_{ps}}$, to the Hamiltonian.

Since $\hat{V_{ps}}$ is not a conventional potential, it is referred to as a pseudopotential that is, a function that depends on the position r. It is important to note that the operator $\hat{V_{ps}}$ is energy-dependent because it varies with ε_v, and it is nonlocal because it depends on the wave function $|\psi_v\rangle$.

Since the energies of valence electrons are always higher than those of the core electrons (i.e., $\varepsilon_v > \varepsilon_c$), the second term in Equation (II.20) is always positive. Because $V(r)$ is an attractive potential, the first term is negative, and it is partially offset by the positive contribution of the second term.

The pseudopotential interacts differently with wave functions of varying angular momentum, reflecting its dependence on energy. The most general form of such a pseudopotential is given by:

$$V_{ps}(r) = \sum_{\ell=0}^{\infty} \sum_{m=-\ell}^{\ell} V_{\ell}^{PS}(r) |\ell m\rangle \langle \ell m| = \sum_{\ell=0}^{\infty} V_{\ell}^{PS}(r)\, \hat{P}_{\ell} \quad \text{(II.24)}$$

Where $|\ell m\rangle$ are the spherical harmonics, $\langle r|\ell m\rangle = Y_{\ell m}(\theta,\phi)$, V_{ℓ}^{PS} is the pseudopotential corresponding to the angular component ℓ, and the operator $Pl = \Sigma|\ell m\rangle\langle \ell m|$ (with m ranging from $-\ell$ to ℓ) is a projection operator onto the ℓth angular momentum subspace.

The expression for V_{ℓ}^{PS} in Equation (II.24) means that when the V_{ℓ}^{PS} operator acts on the electronic wave function, the projection operator P_l selects the different angular momentum components of the wave function, which are then multiplied by the corresponding pseudopotential V_{ℓ}^{PS}. Then, the contributions from all the angular momenta are summed to form the total pseudopotential contribution to the Hamiltonian matrix elements that enter the Schrödinger equation.

Since V_{ℓ}^{PS} acts as a local operator in the radial coordinates depending on ℓ, it can be referred to as an angular-dependent or semi-local pseudopotential. A local pseudopotential is a function that depends solely on the distance from the nucleus [26].

The work of Phillips and Kleinman first laid the theoretical foundation for the pseudopotential method, which can generally be categorized into two types: norm-conserving pseudopotentials and ultra-soft pseudopotentials.

II.6.3.2 Norm conserving pseudopotentials

II.6.3.2.1 Concept of Norm conserving pseudopotentials

A significant advancement in the efforts to produce transferable first-principles pseudopotentials came with the introduction of norm-conserving pseudopotentials by Hamann, Schlüter, and Chiang [27] in 1979, and further developed by Kleinman and Bylander [28]. In this approximation, the all-electron and pseudo wave functions must have the same norm within the ionic core region, defined by a specific radius called the cut-off radius r_c, to ensure that both wave functions generate identical electron densities in the outer region. The pseudo and all-electron wave functions are identical outside the core radius, but differ within the ionic core region defined by the cut-off radius r_c. The charge conservation property of norm-conserving pseudopotentials simplifies their application, making them more accurate and transferable. They can be used to predict the physicochemical properties of an atom in a wide range of situations (volume, surface, etc.). However, the use of norm-conserving pseudopotentials is computationally expensive due to the requirement of norm conservation below r_c. They require large plane-wave basis sets or a high energy cut-off for elements with strongly localized orbitals, such as transition metals and rare earths, thus demanding significantly more computational effort.

II.6.3.2.2 The construction of the norm-conserving pseudopotential

The construction of a pseudopotential from first principles is considered an inverse problem. However, there are fundamental guidelines that assist in solving it. Below is a brief overview of the main steps of the construction, initially formulated by Hamann et al [27]. and later utilized by Bachelet, Hamann, and Schlüter (BHS) [29], who applied this approach to all elements from hydrogen to plutonium.

The process of constructing a norm-conserving pseudopotential includes the following steps:

First, the true radial wave function $R_{n\ell}(r)$ of the atom is obtained by solving the Kohn-Sham radial equation.

$$\left[-\frac{1}{2r}\frac{\hbar^2}{m_e}\frac{d^2}{dr^2}r+\frac{\hbar^2}{2m_e}\frac{\ell(\ell+1)}{r^2}+v(r)\right]R_{n\ell}(r)=e_{n\ell}R_{n\ell}(r) \quad \text{(II.25)}$$

Where

$$V(r)=-\frac{1}{r}+V_H(r)+V_{XC}(r) \quad \text{(II.26)}$$

Here, $V_{XC}(r)$ is the exchange-correlation potential, and $V_H(r)$ is given by:

$$V_H(r)=\int\frac{\rho(r')}{|r-r'|}d^3r' \quad \text{(II.27)}$$

Where $\rho(r')$ is the total electron density.

Once the true radial wave function $R_{n\ell}(r)$ is obtained, we select a cut-off radius r_c (usually between the outermost node and the outermost extremum of the all-electron radial wave function) to construct a pseudo-radial function $R_{n\ell}{}^{ps}(r)$ that satisfies five general criteria:

- The pseudowave function must match the true valence wave function beyond the chosen cut-off radius:

$$R_{n\ell}^{ps}(r)=R_{n\ell}(r) \text{ pour } \quad r\geq r_c\,) \quad \text{(II.28)}$$

-The pseudowave function $R_{n\ell}{}^{ps}(r)$ must be node-free and continuous at re, as well as its first and second derivatives. Since the pseudowave function is constructed only for valence electrons, the principal quantum number n is omitted.

- The normalized atomic radial pseudowave function $R_{n\ell}{}^{ps}(r)$ and the normalized radial true wave function $R_{n\ell}(r)$ must be identical beyond a suitably chosen cut-off radius r_c

$$\left|R_{n\ell}^{ps}(r)\right|^2=|R_{n\ell}(r)|^2 \text{ pour } \quad r\geq r_c \quad \text{(II.29)}$$

The pseudowave function must yield the same energy eigenvalues as the true (all-electron) wave function when solving the Schrödinger equation.

-The amount of charge (or electron density) enclosed within the cutoff radius r_c must be identical for both the pseudowave function and the true wave function, ensuring they represent the same physical behavior in that region.

$$\int_0^{r_c} \left|R_{n\ell}^{ps}(r)\right|^2 r^2 dr = \int_0^{r_c} |R_{n\ell}(r)|^2 r^2 dr \quad \text{(II.30)}$$

The last condition is often known as the norm-conservation condition, and if a pseudopotential satisfies this condition, it is referred to as a Norm-Conserving Pseudopotential (NCPP). It's important to note that a pseudowave function meeting these conditions can be constructed in many different ways, providing considerable flexibility in its design. This flexibility is typically used to create a smoother and more computationally efficient pseudopotential. Once the form of the pseudowave function is defined, the corresponding screened pseudopotential can be obtained by inverting the radial Schrödinger equation (Equation II.26).

$$V_{\ell Sc}^{Ps}(r) = e_{n\ell} - \frac{\ell(\ell+1)}{2r^2} + \frac{1}{2rR_\ell^{PS}} \frac{d^2}{dr^2}\left[rR_\ell^{PS}(r)\right] \quad \text{(II.31)}$$

The pseudopotential $V_{\ell Sc}^{Ps}(r)$ is called "screened" because it includes the effects of the nucleus as well as all electrons, including the valence electrons not just the core electrons. However, this screened pseudopotential lacks transferability, meaning it cannot be reliably used across different chemical environments, since the screening effect from the valence electrons depends heavily on the surrounding environment.

To make the pseudopotential more general and transferable, an "ionic" or "unscreened" version is created one that does not depend on the specific chemical context. This is done through an "unscreening" process, where the contributions from the valence electrons are removed. Specifically, the Hartree and exchange–correlation potentials generated by the pseudo valence electron density are subtracted from the screened pseudopotential. The resulting unscreened pseudopotential reflects only the interaction of the valence electrons with the nucleus and the core electrons, independent of the chemical environment. To make the pseudopotential more transferable and independent of the surrounding environment in other words, to obtain an ionic (unscreened) pseudopotential a process called by removing the effect of the valence electrons, we obtain an "ionic" or "unscreened" pseudopotential that is not influenced by the surrounding chemical environment. This type of pseudopotential is more general and can be applied across various situations whether the atom is isolated, part of a molecule, in a solid, or in a liquid.

Therefore, the ionic pseudopotential we aim to construct is highly transferable and is expressed by the following relation:

$$V_\ell^{PS}(r) = V_{\ell,sc}^{PS}(r) - \int dr' \frac{\rho_v^{PS}(r')}{|r-r'|} - V_{XC}[\rho_v^{PS}(r)] \quad \text{(II.32)}$$

With

$$\rho_v^{PS}(r) = \sum_{\ell m}^{occ} \left| r R_\ell^{PS}(r) \right|^2 \quad \text{(II.33)}$$

When the ionic pseudopotential is used in a new environment, the Hartree potential $V_H(r)$ and the exchange–correlation potential $V_{xc}(r)$ are recalculated based on that specific environment and then added back to the total potential.

However, this does not guarantee that the pseudopotential will be transferable to any environment. It can only be reliably used in systems where the eigenvalues (energy levels) do not differ significantly from those used during its construction.

The characteristic that helps extend the range of energy over which the pseudopotential remains accurate is commonly referred to as smoothness. The smoother the pseudopotential, the less sensitive it is to changes in energy which improves its transferability.

Norm-conserving pseudopotentials, constructed using equation (III.30), generally take a semi-local form. This means that while the potentials are local with respect to the radial coordinate r, they exhibit non-local dependence on the angular variables.

Due to the orbital angular momentum, each angular momentum component of the wave function "experiences" a different potential [30]. The resulting ionic pseudopotential can be expressed in the following form [31]:

$$V^{PS} = \sum_{\ell=0}^{\infty} V_\ell^{PS} \hat{P}_\ell \quad \text{(II.34)}$$

The operator P^ℓ is defined in equation (II.23).

Generally, the non-local pseudopotential can be written in a semi-local form, meaning it is local with respect to the radial coordinate r, but varies with the angular momentum quantum number ℓ, making it non-local overall [26]:

$$\begin{aligned} V^{PS}(r) &= \sum_{\ell=0}^{\infty} V_{loc}^{PS}(r)\hat{P}_\ell + \sum_{\ell=0}^{\ell max} \left[V_\ell^{PS}(r) - V_{loc}^{PS}(r) \right] \hat{P}_\ell \\ &= \sum_{\ell=0}^{\infty} V_{loc}^{PS}(r)\hat{P}_\ell + \sum_{\ell=0}^{\ell max} \left[\Delta V_\ell^{PS}(r) \right] \hat{P}_\ell \end{aligned} \quad \text{(II.35)}$$

With

$$\Delta V_\ell^{PS}(r) = V_\ell^{PS}(r) - V_{loc}^{PS}(r) \quad \text{(II.36)}$$

Here, $V_{loc}^{PS}(r)$ and $\Delta V_\ell^{PS}(r)$ represent the local and semi-local potentials, respectively.

The semi-local potential in equation (II.36) can be transformed into a completely non-local form using a general approach suggested by Kleinman-Bylander (KB) [28] as follows:

$$V_{PP}^{KB} = V_{loc}^{PS} + \sum_{l,m} \frac{|\Delta V_\ell^{PS} \psi_{lm}^{PS}\rangle\langle\psi_{lm}^{PS} \Delta V_\ell^{PS}|}{\langle\psi_{lm}^{PS}|\Delta V_\ell^{PS}|\psi_{lm}^{PS}\rangle} \quad \text{(II.37)}$$

The function $\psi_{\ell m}^{PS}$ represents a specific eigenstate of the atomic pseudo-Hamiltonian.

The operator V_{PP}^{KB} acts on the reference state in the same way as the original semi-local operator $V^{PS}(r)$, making it theoretically well-justified and equivalent in effect.

The key advantage of this form is that the number of required projections scales linearly with the number of basis functions, whereas for the semi-local form, it scales quadratically.

This separable form can thus be viewed as a kind of "correction" to the local pseudopotential in the core region.

II.6.3.3 Vanderbilt Pseudopotential (Ultrasoft)

II.6.3.3.1 Concept of Vanderbilt Pseudopotential (Ultrasoft)

David Vanderbilt extended the concept of "norm-conserving pseudopotentials"[32] by developing what are known as ultra-soft pseudopotentials. In this approach, Vanderbilt [32] demonstrated that it is possible to create non-norm-conserving pseudopotentials that are still highly transferable by relaxing the norm-conservation constraint, which is the main factor making norm-conserving pseudopotentials difficult to use. The only remaining constraint is the matching of the pseudo and all-electron wave functions for $r \geq r_c$, which allows for the selection of a much larger value for rc. As a result, the kinetic energy is reduced, the valence electrons experience a smoother potential, and the number of plane waves required to describe the system decreases. This is why Vanderbilt's ultra-soft pseudopotentials are among the most widely used in the condensed matter community. Pseudopotentials can be softened further by increasing the cutoff radius, but there is an upper limit to this increase; if the cutoff radius is extended beyond this limit, the transferability of the pseudopotential is reduced. Relaxing the norm-conserving constraint causes a charge-density deficit between the pseudo and exact wave functions, which must be accounted for when generating the ultra-soft pseudopotential. This can be handled by splitting the pseudo wave functions into two parts: the ultra-soft valence wave function, which does not satisfy the norm-conservation criteria, and the core augmentation charge functions, which represent the charge density difference between the all-electron and pseudo wave functions and are strictly localized in the core region.

$$Q_{nm}(r) = \psi_n^*(r)\psi_m(r) - \psi_n^{pp*}\psi_m^{pp} \quad \text{(II.38)}$$

Therefore, the norm-conservation condition will be fulfilled when $Q_{nm}(r) = 0$.

II.6.3.3.2 The construction of ultrasoft potentials

The generation of ultrasoft potentials starts in the same way as norm-conserving pseudopotentials. For a given species, the atomic Kohn-Sham system is solved self-consistently, resulting in the screened all-electron potential, V_{AE}. Then, for each angular momentum channel, a few energy values, τ, are selected (τ being the number of such energies, usually a maximum of 3). For the already obtained V_{AE}, the Schrödinger equation is then solved.

$$[T + V_{AE}]|\psi_n\rangle = \varepsilon_n|\psi_n\rangle \quad \text{(II.39)}$$

Here, n is a composite index that includes ll for the angular momentum quantum number, m for the projection, and τ. So, n={τlm}.

Next, three cutoff radii are chosen as follows:

1 -A smooth local (ℓ-independent) potential is created that matches V_{AE} after the radius r_c^{loc}.

2 -A second cutoff radius r_{cl} is chosen for each angular momentum channel, and a pseudofunction, ψ_n^{pp} is constructed that matches the real wave function $|\psi_n\rangle$ at r_{cl}.

3 -Finally, a diagnostic radius R is selected such that it is slightly larger than the maximum of all the radius r_c^{loc} and $r_{cl,}$ ensuring that all quantities of the pseudopotential (PS) and all-electron (AE) agree beyond R_c.

Then, a smooth pseudofunction wave is determined for each angular momentum channel, with the condition that it matches the real wave functions outside the chosen cutoff radius r_{cl} .

Next, the Kohn-Sham equations are inverted to obtain the total effective V_{KS}^{PP} pseudopotential that satisfies the following equations:

$$\left(\hat{T} + V_{eff}^{ps}\right)\psi_n^{pp} = \varepsilon_n\psi_n^{pp} \quad \text{(II.40)}$$

The total effective pseudopotential is then divided into local and non-local contributions.

$$V_{KS}^{PP} = V_L + V_{NL} \quad \text{(II.41)}$$

The local potential V_L is chosen to be smooth, and this potential matches the all-electron potential beyond the chosen cutoff radius rc. By inserting equation (II.42) into equation (II.39), we can construct the following orbital for each pseudofunction wave [33]:

$$|\chi_n\rangle = \left[\varepsilon_n - T - \hat{V}_L\right]\left|\psi_n^{pp}(r)\right\rangle \quad \text{(II.42)}$$

The orbitals $|\chi_n\rangle$ are local and vanish beyond the radius R, where $V_{lo}=V_{AE}$ and $\psi_n^{PP}=\psi_n$. Then, an auxiliary matrix of inner products is calculated.

$$(B^{-1})_{mn} = \langle\psi_n^{pp}|\chi_m\rangle \quad \text{(II.43)}$$

The projectors required to define the non-local part of the potential are defined as follows:

$$|\beta_n\rangle = \sum_n|\chi_n\rangle\langle\chi_m|\psi_n^{pp}\rangle = \sum_n(B^{-1})_{mn}|\chi_m\rangle \quad \text{(II.44)}$$

The total non-local operator is then expressed as follows:

$$\hat{V}_{NL} = \sum_{n,m} B_{nm} |\beta_n\rangle\langle\beta_m| \quad \text{(II.45)}$$

Provided that the norm-conserving constraint of the pseudo-wave function is adhered to. Norm-conservation will be satisfied when:

$$Q_{nm}(r) = \psi_n^*(r)\psi_m(r) - \psi_n^{pp*}\psi_m^{pp} = 0 \quad \text{(II.46)}$$

We note that in the special case where a single reference energy is chosen for each angular momentum, equation (III.42) simply reduces to the Kleinman-Bylander form of the separable non-local potential [33]. Vanderbilt has shown that the norm-conserving constraint in equation (II.44) can be relaxed by introducing a generalized Hermitian overlap operator S:

$$S = 1 + \sum_{nm} q_{nm} |\beta_n\rangle\langle\beta_m| \quad \text{(II.47)}$$

Therefore, the orthonormality condition that must be satisfied in the solution of the Kohn-Sham equations is:

$$\langle\psi_n|S|\psi_m\rangle = \delta_{nm} \quad \text{(II.48)}$$

In equation (II.45), q_{nm} is the integral of the augmentation function $Q_{nm}(r)$ over the spherical region defined by r_c:

$$q_{nm} = \int dr\, Q_{nm}(r) \quad \text{(II.49)}$$

The new non-local operator V_{NL} takes the form:

$$V_{NL} = \sum_{nm} D_{nm} |\beta_n\rangle\langle\beta_m| \quad \text{(II.50)}$$

Where the new coefficients are:

$$D_{nm} = B_{nm} + \varepsilon_m q_{nm} \quad \text{(II.51)}$$

With all these descriptions, we can verify that the pseudo functions satisfy the equation.

$$\left(\hat{T} + V_{loc} + \sum_{nm} D_{nm} |\beta_n\rangle\langle\beta_m|\right)|\psi_n^{pp}\rangle = \varepsilon_i(1 + \sum_{nm} q_{nm} |\beta_n\rangle\langle\beta_m|)|\psi_n^{pp}\rangle)$$

$$\left(\hat{T} + V_{loc} + \sum_{nm} D_{nm} |\beta_n\rangle\langle\beta_m|\right)|\psi_n^{pp}\rangle = \varepsilon_i S|\psi_n^{pp}\rangle \quad \text{(II.52)}$$

It can be verified that the ultrasoft pseudopotentials generated with the above steps exhibit excellent transferability; this means that the pseudo-wave functions and their logarithmic

derivatives correspond to each reference energy and for small variations around it. To compensate for the charge deficit, the valence charge density is defined as:

$$\rho(r) = \sum_n \left[|\psi_n^{ps}(r)|^2 + \sum_{i,j} Q_{ji}(r)\langle\psi_n^{ps}|\beta_i\rangle\langle\beta_j|\psi_n^{ps}\rangle\right] \quad \text{(II.53)}$$

II.7 Resolution of Kohn-Sham equations

To set up and solve the Kohn-Sham equations, we need to define both the Hartree operator V_H and the exchange-correlation operator V_{xc}, which depend on the density ρ(r). However, to

construct the electron density, we must know the single-electron wave functions, and to find these wave functions, we need to solve the Kohn-Sham equations. This means that the estimated solution of the Kohn-Sham problem must be known before it can be solved, so an iterative procedure is required to overcome this paradox (see Figure II.2). The Kohn-Sham equations for the system can be constructed for a trial electron density and a given set of atomic coordinates. The system's geometry for density functional calculations is constructed using experimental data such as bulk lattice constants, previous first-principles calculations, semi-empirical methods, or from intuition. Once the trial electron density is defined, Poisson's equation is set up and solved to obtain the electrostatic Coulomb potential. The explicit form of the exchange-correlation potential is then used, and the exchange-correlation operator is constructed. All of these terms are combined to give the full Hamiltonian in equation:

$$\left[-\frac{1}{2}\nabla^2 + V_{eff}\right]\psi_i(r) = \varepsilon_i\psi_i(r) \qquad \text{(II.54)}$$

Using standard mathematical techniques for solving eigenvalue problems, the unknown solutions $\psi_i(r)$ of equation:

$$\left[-\frac{1}{2}\nabla^2 + V_{eff}\right]\psi_i(r) = \varepsilon_i\psi_i(r) \qquad \text{(II.55)}$$

for each k-point can be expanded in a set of known functions $\phi_j(r)$, with unknown linear coefficients c_{ij}.

$$\psi_i(r) = \sum_j c_{ij}\phi_j(r) \qquad \text{(II.56)}$$

There are many possible choices for the basis set, although Gaussians have dominated the molecular community, while plane waves have been the de facto standard in solid-state physics. In principle, $\phi_j(r)$ has infinite dimensions, but in practice, a limited set of basis functions is used to generate a function that is "close" to $\phi_j(r)$ using the technique discussed in section (II.4).

The coefficients that determine how much these functions contribute to the development of the Kohn-Sham function are found by constructing the energy functional (i.e., the expectation value of the Hamiltonian) and applying the Variational principle. This transforms the partial differential equation into a discrete matrix problem that can then be solved.

$$\sum\left[\langle\phi_{ik}|H|\phi_{jk}\rangle - \varepsilon_{nk}\langle\phi_{ik}|\phi_{jk}\rangle\right]c_{ink} = 0$$

$$\sum\left[H_{ij} - \varepsilon_{nk}\,S_{ij}\right]c_{ink} = 0 \qquad \text{(II.57)}$$

With

$$H_{ij} = \langle\phi_{ik}|H|\phi_{jk}\rangle \qquad \text{(II.58)}$$

And

$$S_{ij} = \langle \phi_{jk} | \phi_{ik} \rangle \quad \text{(II.59)}$$

Where H_{ij} are the matrix elements of the Kohn-Sham Hamiltonian in the basis states, and S_{ij} are the matrix elements of the overlap.

Diagonalizing the matrix (II.57) at each k-point yields a set of eigenvalues for the particle and the variational expansion coefficients corresponding to each eigenvalue. In principle, the initial wave functions at each k-point in the irreducible wedge of the Brillouin zone can be obtained using the expansion coefficients. The occupation of each state is determined using Fermi-Dirac statistics, which means that the eigenvalues are generated in increasing energy, and all states are filled until the total number of electrons in the system is exhausted.

The electron density at a specific point k is thus:

$$\rho^k(r) = \sum_{i=1}^{N} |\phi_i^k|^2 \quad \text{(II.60)}$$

Therefore, the new total electron density ("output") can be calculated by summing the densities at the sampled k-points.

$$\rho(r) = \frac{\Omega}{(2\pi)^3} \sum_{k}^{1^{eme}Bz} \rho^k(r)\, \Delta k \quad \text{(II.61)}$$

Where Δk is the sampling spacing for the k-points, which can be manually determined. It is clear that the smaller Δk is selected, the more accurate the calculation of ρ(r) will be. However, as the number of electrons in the system increases, the computational cost will also rise, making it nearly impossible to solve systems with a large number of electrons. The generated electron density is called the output electron density. If the output electron density does not equal the input density, it will be used as the input for the next iteration, and this process is repeated multiple times until the newly evaluated electron density matches the old one. This is known as the self-consistent field (SCF) cycle. In practice, the process is iterated for a sufficient number of times until the residual difference between the input and output densities does not cause significant errors in the total energy or other properties of interest. The resulting electron density also corresponds to the ground-state density, as it is the only density that can be correctly solved from the Kohn-Sham equation.

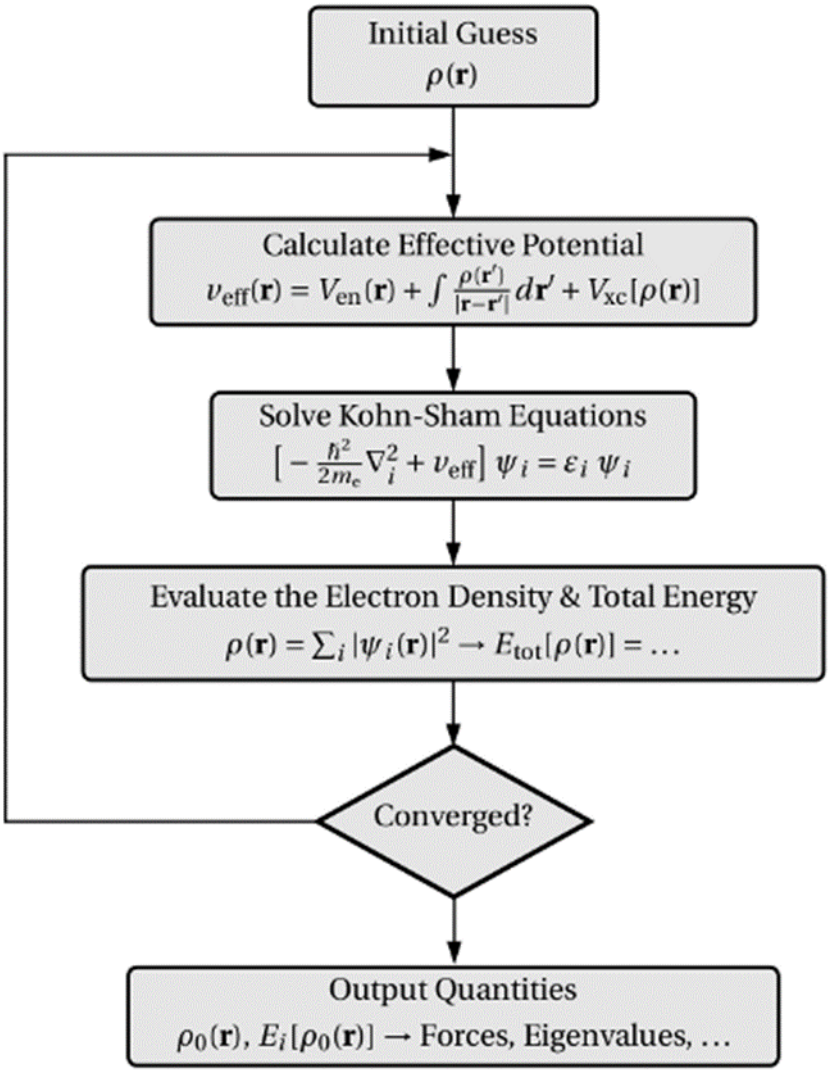

Fig. II.2: A flowchart of a typical DFT calculation using the Kohn-Sham method.

References

[1] E. Kaxiras, Atomic and Electronic Structure of Solids, Cambridge University Press, Cambridge (2003).

[2] N.W. Ashcroft, N.D. Mermin: Solid State Physics, Holt Rinehart and Winston, New York (1976).

[3] F. Bloch, Z. Physik 52, 555 (1928).

[4] M. C. Payne, M. P. Teter, D. C. Allan, T. A. Arias, and J. D. Joannopoulos, Rev. Mod. Phys. 64, 1045 (1992).

[5] J. Ihm, A. Zunger, M.L. Cohen, J. Phys. C 12, 4409 (1979).

[6] D. S. Sholl and J. A. Steckel, Density Functional Theory: A Practical Introduction, John Wiley & Sons, Hoboken, New Jersey (2009).

[7] L. P. Bouckaert, R. Smoluchowski, and E. Wigner. Phys. Rev. 50, 58 (1936).

[8] D. J. Chadi and M. L. Cohen, Phys. Rev. B 8, 5747 (1973).

[9] J. D. Joannopoulos and M. L. Cohen, J. Phys. C 6, 1572 (1973).

[10] R.A. Evarestov and V.P. Smirnov, Phys. Status Solidi 119, 9 (1983).

[11] H. J. Monkhorst and J. D. Pack, Phys. Rev. B 13, 5188 (1976).

[12] R. M. Martin, "Electronic Structure Basic Theory and Practical Methods," Cambridge University Press, Cambridge, (2004).

[13] W. E. Pickett, Comput. Phys. Rep. 9, 115 (1989).

[14] U. von Barth and C. D. Gelatt, Phys. Rev. B 21, 2222 (1980).

[15] S. Goedecker and K. Maschke, Phys. Rev. A 45, 88 (1992).

[16] V. Heine. The pseudopotential concept. In Solid State Physics, Vol. 24, Academic Press, New York (1970).

[17] W. E. Pickett, Comp. Phys. Rep. 9, 115 (1989).

[18] M. L. Cohen and V. Heine. The fitting of pseudopotentials to experimental data and their subsequent application, volume 24 of Solid State Physics. Academic Press, New York, (1970). [19] M.L. Cohen, J.R. Chelikowsky, Electronic Structure and Optical Properties of Semiconductors, Springer, Berlin, (1988).

[20] W. A. Harrison, "Pseudopotentials in the Theory of Metals, Benjamin, New York, (1966).

[21] B. J. Austin, V. Heine and L. J. Sham, Phys. Rev. 127, 276 (1962).

[22] R.W. Shaw, Jr. and W.A. Harrison, Phys. Rev. 163, 604 (1967).

[23] E. Fermi, Nuovo Cimento 11, 157 (1934).

[24] J. C. Phillips, Phys. Rev. 112, 685 (1958).

[25J. C. Phillips and L. Kleinman, Phys. Rev. 116, 287 (1959).

[26] J. Kohanoff, Electronic structure calculations for solids and molecules: theory and computational methods, Cambridge University Press, New York (2006).

[27] D. H. Hamann, M. Schlüter, and C. Chiang, Phys. Rev. Lett. 43, 1494 (1979).

[28] L. Kleinman and D. M. Bylander, Phys. Rev. Lett. 48, 1425 (1982).

[29] G. B. Bachelet, D. R. Hamann, and M. Schlüter, Phys. Rev. B 26, 4199 (1982).

[30] N. Troullier and J. L. Martins, Phys. Rev. B 43, 1993 (1991)

[31] X. Gonze, R. Stumpf, and M. Scheffler, Phys. Rev. B 44, 8503 (1991).

[32] D. Vanderbilt, Phys. Rev. B 41, 7892 (1990).

[33] G. Kresse and J. Hafner, J. Phys. Condens. Matter 6, 8245 (1994).

CHAPTER III

RESULTS AND DISCUSSIONS

III.1. **Computational details**

In order to benefit of the advantages of available computational methods, two complementary first-principles approaches in the framework of density functional theory (DFT) were used to perform a complete investigation of the structural, electronic and optical properties of these three lead-free halide perovskites ($AgXBr_3$, X = Ca, Sr, Ba).

We have employed the first-principles pseudopotential plane-wave (PP-PW) method as implemented in the Cambridge Serial Total Energy Package (CASTEP) code [1] to determine the structural parameters. A new version of the generalized gradient approximation (GGA), namely the GGA-PBEsol [2], which has been developed specifically to improve the description of the exchange-correlation in solids, was used. Interactions of the valence electrons with the nucleus and frozen core electrons were modelled using Vanderbilt ultrasoft pseudopotentials [3]. The Ag: 4d105s1, Ca: 3s23p64s2, Sr: 4s24p65s2, Ba: 5s25p66s2, and Br: 3d104s24p5 electrons were treated as valence states. Valence electronic wave functions were expanded in a plane wave basis set truncated at maximum plane-wave energy (the cut-off energy) of 600 eV. The Brillouin zone (BZ) was sampled on a 9 × 9 × 9 Monkhorst–Pack special k-mesh [4]. The self consistent calculations were considered to converge when the difference in the total energy was within 5.0 × 10−7 eV/atom. Very careful step analysis is done to ensure convergence of the total energy, lattice parameters and optical properties in terms of the variational cut-off energy and number of k-points in the Brillouin zone. We have verified that further increase in the energy cut-off and k-point number did not lead to any noticeable changes in the total energy. We have also experimented with the basis set cut-off and number of k-points that at the equilibrium volume the cut-off energy of 600 eV and 9 × 9 × 9 Monkhorst–Pack special k-mesh were sufficient in the sense that the predicted lattice parameters did not change noticeably when we increased the number of basis functions and k-point number. For optical properties, since the imaginary part of the dielectric function is usually calculated first, we choose it as a reference for the assessment of convergence. In optical calculations, a 21 × 21 × 21 Monkhorst–Pack k points sampling is found to be enough to get convergence value.

The geometry optimization of all free lattice parameters and internal coordinates was determined using the Broyden–Fletcher–Goldfarb–Shanno minimization technique [BFGS] [5], which is known to provide a fast way to find the lowest energy structure. The optimization was performed until the forces on the atoms were less than 0.01 eV/A, all the stress components were less than 0.02 GPa and the tolerance in the self-consistent field (SCF) calculations was 5.0 × 10−7 eV/atom.

III.2. **Results and discussion**

III.2.1 **Structural properties**

The perovskite materials $AgXBr_3$ (X = Ca, Sr, and Ba) have a simple cubic crystal structure, characterized by the space group $Pm\bar{3}m$ (#221) [6]. The unit cell comprises one chemical formula unit (Z = 1). The atomic positions within the unit cell are as follows: Ag occupies the Wyckoff site 1a (0, 0, 0), X (X = Ca, Sr, and Ba) resides in the Wyckoff site 1b (1/2, 1/2, 1/2), and Br is located in the Wyckoff site 3c (1/2, 1/2, 0). Fig. 1 depicts the prototype unit cell of $AgCaBr_3$. The Ca cation is coupled with six Br anions, resulting in the formation of regular octahedra $CaBr_6$, and Ag cation exhibit coordination with twelve bromine anions, resulting in the formation of cuboctahedral coordination environments. To ascertain the lattice parameter (a), bulk modulus (B), and its pressure derivative (B') for the considered compounds, we employed the Birch and Birch-Murnaghan equations of state (EOS) [7] to fit the calculated total energy (E) against the unit cell volume (V). The calculated values of the equilibrium lattice parameter (a), bulk modulus (B) and its pressure derivative (B') for $AgCaBr_3$, $AgSrBr_3$, and $AgBaBr_3$ are listed in Table 1. It is observed that the lattice parameter values, exhibit a satisfactory level of concurrence with the existing data documented in the literature [6]. It is worth mentioning that the lattice parameter of $AgXBr_3$ increases as the atomic size of X element increases. A comparison of the bulk modulus values listed in Table 1 for the three compounds studied shows that they decrease when moving from $AgCaBr_3$ to $AgSrBr_3$ and then to $AgBaBr_3$. This trend suggests that the hardness of these compounds decreases slightly when moving from $AgCaBr_3$ to $AgSrBr_3$ and then to $AgBaBr_3$. We note that the values of B acquired by the two equations of state, namely Birch and Birch-Murnaghan EOS (Fig. 2), are in excellent agreement, indicating the reliability of the results obtained.

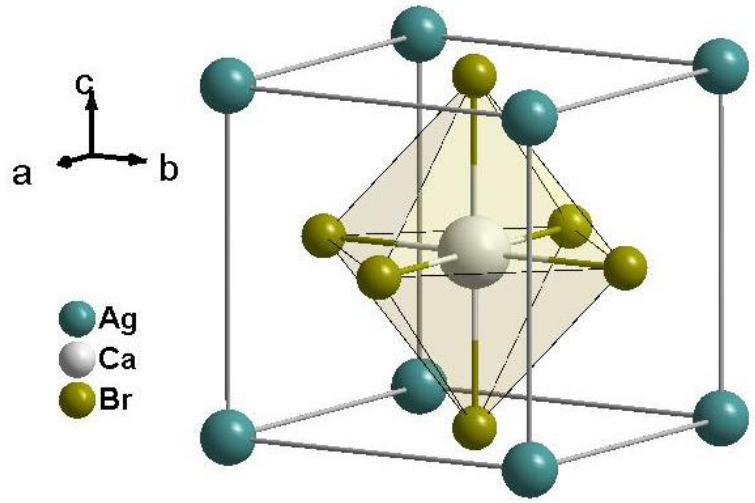

Fig. 1: Schematic representation of the unit cell of $AgCaBr_3$ showing the $CaBr_6$ octahedron

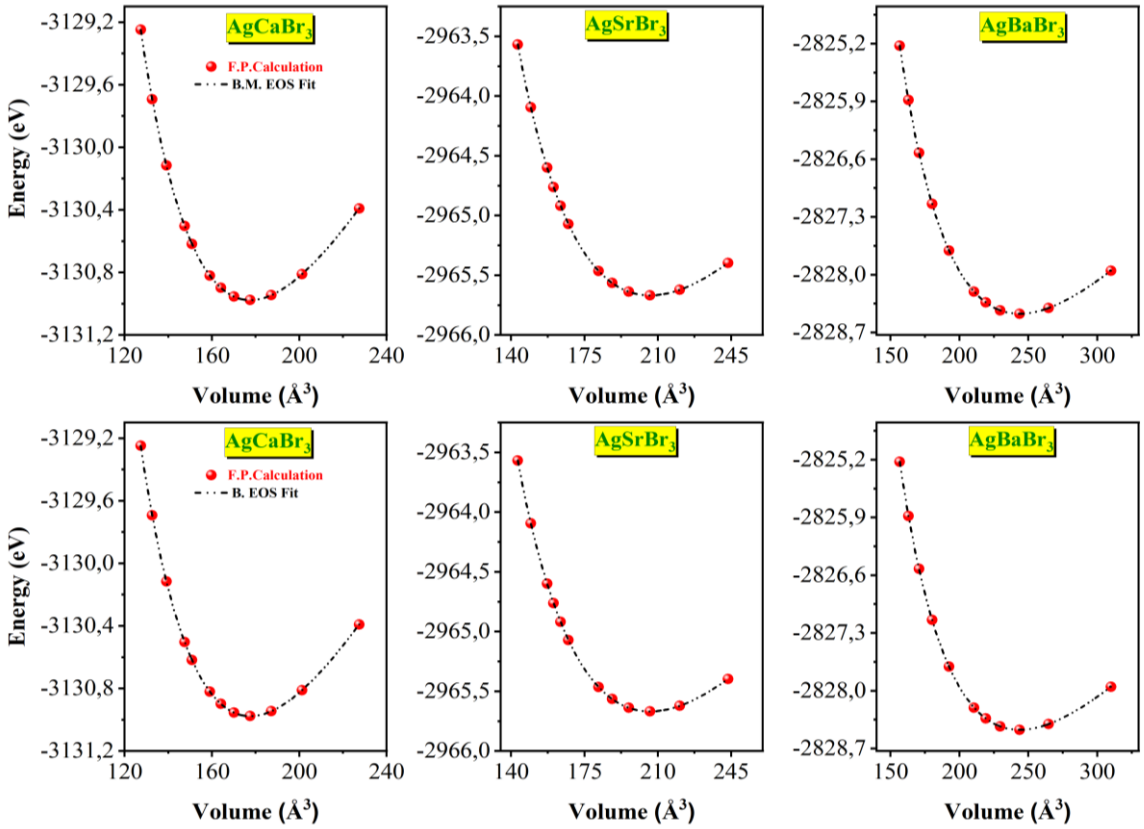

Fig. 2: Energy-volume graphs depicting the relationship between total energy (E) and the volume (V) of the primitive cell for $AgCaBr_3$, $AgSrBr_3$, and $AgBaBr_3$. The symbols represent the results obtained from first-principles calculations (F.P. cal.), whereas the continuous lines correspond to the fits of the E-V data using the Birch and Birch-Murnaghan equations of state (EOS).

To evaluate the stability of the materials under consideration with the cubic structure, we computed the Goldsmith tolerance factor (t) [8]. The stability of a cubic perovskite ABX_3 structure is conditioned by values of "t" between 0.8 and 1.0. The Goldschmidt tolerance factor values for $AgCaBr_3$, $AgSrBr_3$, and $AgBaBr_3$, as shown in Table 1, fall within the required values range. This suggests that these materials exhibit stability within the cubic structure.

Furthermore, we calculated the formation enthalpy (ΔH) and cohesive energy (Ecoh) for $AgCaBr_3$, $AgSrBr_3$, and $AgBaBr_3$ in order to assess their structural and thermodynamic stabilities [9–13]. The formation enthalpies and cohesive energies of the compounds $AgXBr_3$ (X = Ca, Sr and Ba) were calculated using the subsequent relationships:

$$\Delta H = \frac{1}{n_{Ag} + n_X + n_{Br}} \left[E_{tot}^{AgXBr_3} - \left(n_{Ag} E_{tot}^{Ag(solid)} + n_X E_{tot}^{X(solid)} + n_{Br} E_{tot}^{Br(solid)} \right) \right]$$

$$E_{coh} = \frac{1}{n_{Ag} + n_X + n_{Br}} \left[E_{tot}^{AgXBr_3} - \left(n_{Ag} E_{tot}^{Ag(atom)} + n_X E_{tot}^{X(atom)} + n_{Br} E_{tot}^{Br(atom)} \right) \right]$$

Here, $E_{tot}^{AgXBr_3}$ is the total energy of the primitive cell of $AgXBr_3$; $E_{tot}^{Ag(solid)}$, $E_{tot}^{X(solid)}$ and $E_{tot}^{Br(solid)}$ are the total energies per atom of the pure Ag, X (X = Ca, Sr, Ba) and Br elements in their solid state; $E_{tot}^{Ag(atom)}$, $E_{tot}^{X(atom)}$ and $E_{tot}^{Br(atom)}$ are the total energies of the isolated Ag, X, and Br atoms; n_{Ag}, n_X and n_{Br} represent respectively the number of Ag, X, and Br atoms in the primitive cell. The calculated formation enthalpies and cohesive energies for $AgXBr_3$ (X = Ca, Sr, Ba) are given in Table 1. The studied perovskites in their cubic structure are structurally and energetically stable, as evidenced by the negative values of both the formation enthalpies (ΔH) and cohesive energies (E_{coh}). Fig. 3 depicts the fluctuation of ΔH in relation to pressure. It is evident that the value of ΔH remains negative within the specified pressure range, but it rises as the pressure increases. Consequently, the stability of these materials decreases as pressure increases. It is also observed that the stability of $AgXBr_3$ decreases as the cation X moves down the column of the periodic table, in the order: Ca→Sr→Ba.

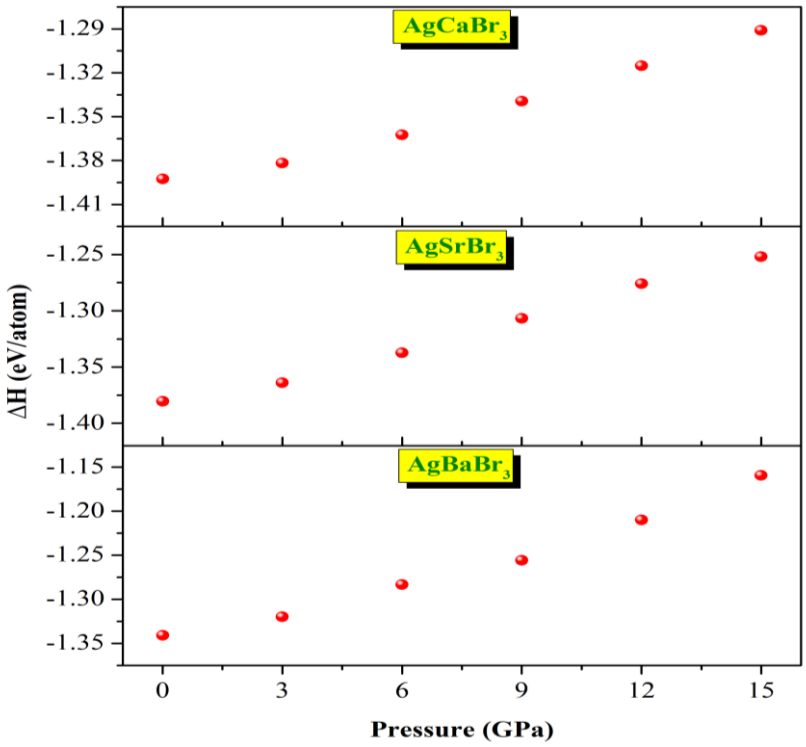

Fig. 3: Pressure dependence of the enthalpy of formation (ΔH) for AgCaBr3, AgSrBr3 and AgBaBr3 materials.

Table 1: Calculated lattice parameter (a0, in Å), Goldschmidt tolerance factor (t), cohesive energy (Ecoh, in eV/atom), formation enthalpy (ΔH, in eV/atom), bulk modulus (B, in GPa), bulk modulus first pressure derivative (B') for the ternary halide perovskites: AgCaBr3, AgSrBr3 and AgBaBr3.

Property	**$AgCaBr_3$**		**$AgSrBr_3$**		**$AgBaBr_3$**	
	GGA	Other [6]	GGA	Other [6]	GGA	Other [6]
a_0	5.6201	5.4815	5.9082	5.7490	6.2453	6.1310
t	0.86		0.80		0.79	
E_{coh}	-1.2288		-1.1965		-1.2014	
ΔH	-1.3925		-1.3803		-1.3409	
B	21.17[1]		17.66[1]		14.62[1]	
	21.17[2]		17.66[2]		14.62[2]	
B'	4.52[1]		4.58[1]		4.63[1]	
	4.53[2]		4.58[2]		4.64[2]	

[1]from Birch E - V EOS; [2] from Birch-Murnaghan E - V EOS.

To assess the dynamical stability of the compounds under scrutiny, we examined their phonon dispersion spectra. This examination was carried out employing the linear response method implemented in the CASTEP code [14]. The resulting phonon dispersion diagrams are visualized in Fig. 4. In materials research, the absence of soft modes (also referred to as imaginary modes or negative frequencies) in the phonon dispersion curve of a material is an indicator of its dynamic stability [15–21]. Theoretically, soft modes represented by negative frequencies in the phonon dispersions of materials indicate their dynamic instability. Such soft modes are known to initiate lattice instability, potentially leading to structural phase transitions. Additionally, their presence suggests that synthesizing the compound under normal conditions may be challenging. It is, however, imperative to emphasize the nuanced nature of the implications associated with the presence of negative frequencies in the phonon dispersion curves of materials. In some cases, this phenomenon does not categorically mean that the crystal structures of these materials are inherently unstable. Indeed, a multitude of previously synthesized materials exhibited soft vibrational modes [22–24], thus demonstrating that a material can maintain its stability even in the presence of these soft modes. Therefore, the mere existence of soft modes within the materials in question should not be automatically interpreted as proof of the impossibility of their synthesis. Further investigations are needed to determine the conditions under which the considered materials can be synthesized and stabilized.

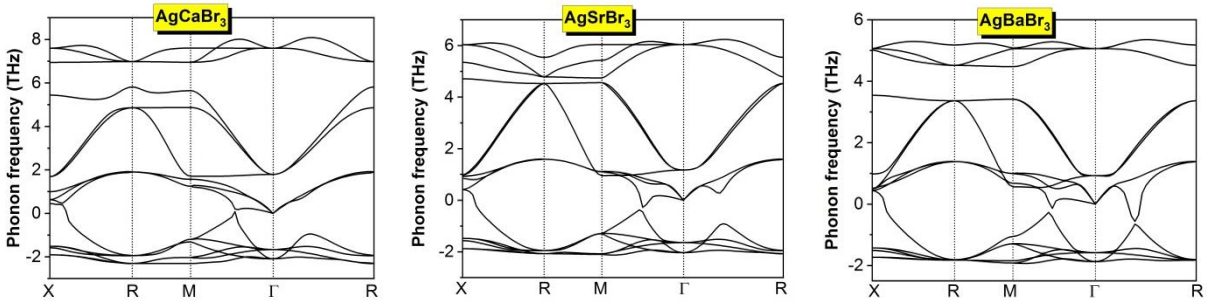

Fig. 4: Phonon dispersion curves for $AgCaBr_3$, $AgSrBr_3$ and $AgBaBr_3$ compounds

To examine the impact of external pressure on the unit cell volume "V" and lattice parameter "a" of the $AgXBr_3$ (X = Ca, Sr, and Ba) materials, we examined a/a0 and V/V0 as functions of pressure as depicted in Fig. 5, where V and a represent the unit cell volume and lattice parameter, respectively, at a pressure P, while V0 and a0 denote their respective values at zero pressure. The calculated a/a0 and V/V0 ratios as functions of pressure were well fitted, as illustrated in Fig. 5, by the following third-order polynomials:

$$\begin{cases} \left(\frac{a}{a_0}\right)^{AgCaBr_3} = 1 - 0.014\,P + 7.41\times10^{-4}P^2 - 1.91\times10^{-5}P^3 \\ \left(\frac{V}{V_0}\right)^{AgCaBr_3} = 1 - 0.040\,P + 2.39\times10^{-3}P^2 - 6.33\times10^{-5}P^3 \end{cases},$$

$$\begin{cases} \left(\frac{a}{a_0}\right)^{AgSrBr_3} = 1 - 0.016P + 9.27\times10^{-4}P^2 - 2.48\times10^{-5}P^3 \\ \left(\frac{V}{V_0}\right)^{AgSrBr_3} = 1 - 0.046P + 2.96\times10^{-3}P^2 - 8.11\times10^{-5}P^3 \end{cases},$$

$$\begin{cases} \left(\frac{a}{a_0}\right)^{AgBaBr_3} = 1 - 0.018P + 1.16\times10^{-3}P^2 - 3.22\times10^{-5}P^3 \\ \left(\frac{V}{V_0}\right)^{AgBaBr_3} = 1 - 0.053P + 3.65\times10^{-3}P^2 - 1.03\times10^{-4}P^3 \end{cases}$$

It is clear from Fig. 5 that both a/a_0 and V/V_0 decrease with increasing pressure for $AgXBr_3$ (X = Ca, Sr, Ba). In addition, it is found that the resistance to both unidirectional and volumetric compression decreases in the order of $AgCaBr_3$, $AgSrBr_3$, and $AgBaBr_3$, with $AgBaBr_3$ being the most compressible.

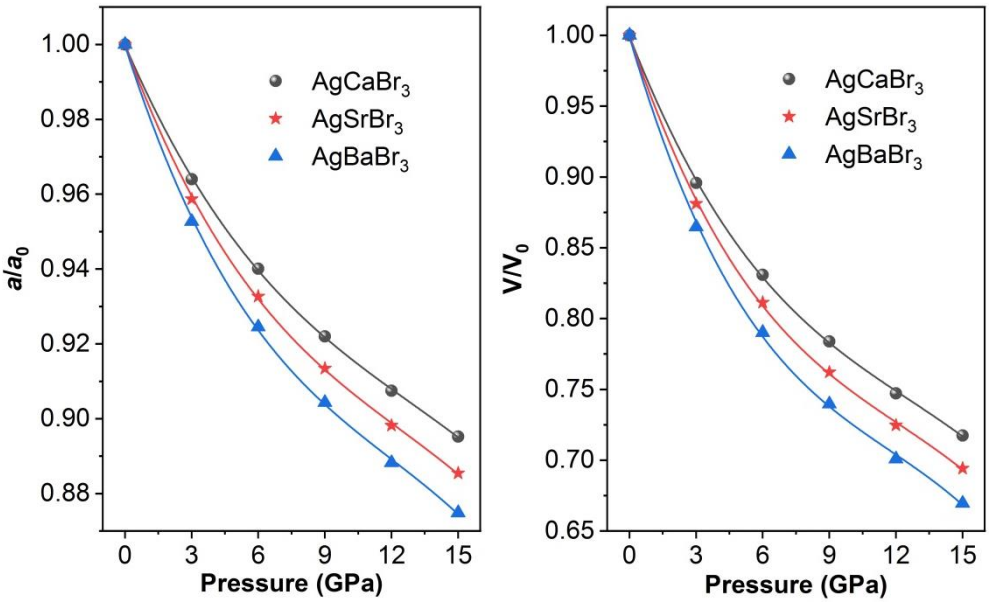

Fig. 5: Pressure dependence of a/a0 and V/V0 for $AgCaBr_3$, $AgSrBr_3$ and $AgBaBr_3$ materials. a and V are the lattice parameter and unit cell volume, respectively, at a pressure P and a0 and V0 are their corresponding values, respectively, at zero pressure.

III.2.2**Electronic properties**

The electronic structure of a substance is intricately linked to several of its physical characteristics, including optical, transport, and thermoelectric characteristics. The electronic band structure and density of states of $AgXBr_3$ (X = Ca, Sr, and Ba) compounds were extensively investigated in this study. The energy band dispersions along the X–R–M–Γ–R path in the first Brillouin zone for the materials under consideration were determined using the GGA PBEsol, TB-mBJ and HSE06 exchange-correlation functionals. Fig. 6 displays the computed energy band dispersions using the GGA-PBEsol and TB-mBJ functionals. The calculated bandgap values for herein studied compounds within the GGA-PBE, TB-mBJ and HSE06 exchange-correlation functionals are listed in Table 2. It is clear from Table 2 that the band gap values obtained using the GGA-PBE exchange-correlation functional are remarkably smaller compared to the corresponding values obtained using the TB-mBJ and HSE06 functionals. It is widely recognized that the GGA functional tends to underestimate the value of the band gap. It is worth mentioning that the band gap values produced using GGA-PBEsol show a higher degree of agreement with those documented in previous studies that used DFT with the GGA functional [6]. The HSE06 exchange-correlation functionals produce significantly improved bandgap values compared to those obtained using GGA-PBEsol. Examination of the calculated band structures determined using the TB-mBJ potential indicates that all three compounds studied have fundamental indirect energy band gaps (Γ–R) of approximately 4 eV, with a slight increase as the atomic size of element X increases from $AgCaBr_3$ to $AgSrBr_3$ to $AgBaBr_3$. Based on the calculated values of the energy bandgaps, these compounds can be classified as wide bandgap semiconductors, and this makes them potential candidates for ultraviolet and visible light emitters, transparent conducting electrode and other optoelectronic applications [24- 26]. It is worth noting that Table 2 and Fig. 7 show that the values of the R–R and X–R energy band gaps, especially that of the X–R band gap, are quite close to that of the fundamental band gap.

To analyze the nature and distribution of the electronic states forming the energy bands of the $AgXBr_3$ compounds, we calculated the total density of states (TDOS) and the partial density of states (PDOS) on specific atomic sites and orbitals within an energy range of -15 to 10 eV. Fig. 8 displays the calculated TDOD and PDOS curves. The obtained DOS diagrams reveal that the characteristics of the DOS spectra of the compounds considered are similar. This similarity can be attributed to the fact that the differing atoms, X (X = Ca, Sr, or Ba), are isoelectronic. Fig. 8 shows that the valence bands of $AgCaBr_3$ are subdivided into two distinct subbands, V_1 and V_2, while for $AgSrBr_3$ and $AgBaBr_3$, the valence bands are subdivided into three band groups: V_1, V_2, and V_3. The lowest energy valence band groups of $AgSrBr_3$ and

$AgBaBr_3$, labeled V_3, exhibit relatively narrow shapes with peaks centered at -15 eV and -12.61 eV, respectively. Similarly, the V_2 valence subband, which also has narrow shapes, shows a peak centered at -12.61 eV for $AgCaBr_3$, -12.17 eV for $AgSrBr_3$, and -9.67 eV for $AgBaBr_3$. All of these valence band groups, namely V2 and V3, are composed of hybridized Br-s and X p (X = Ca, Sr, or Ba) states. The upper valence band groups extend from -2.80 eV, -2.21 eV, and -2.07 eV to the Fermi level (0 eV) for $AgCaBr_3$, $AgSrBr_3$, and $AgBaBr_3$, respectively. This valence subband is mainly formed by the hybridization between the d orbitals of Ag atoms and the p orbitals of Br atoms. The p orbitals of Ca, Sr, and Ba atoms are primarily responsible for the bottom of the conduction band.

Table 2: The predicted values (in eV) of the energy direct bandgap R–R and indirect bandgaps Γ–R and X–R using the GGA-PBEsol, TB-mBJ and HSE06 functionals for $AgCaBr_3$, $AgSrBr_3$ and $AgBaBr_3$ compounds and the relevant theoretical information found in existing literature.

Compound	**XC functional**	***R–R***	***Γ – R***	***X – R***
$AgCaBr_3$	GGA-PBEsol	1.189	0.809	0.823
	TB-mBJ	4.308	3.986	4.002
	HSE06		2.321	
	Other [6]		0.730	
$AgSrBr_3$				
	GGA-PBEsol	1.061	0.790	0.797
	TB-mBJ	4.386	4.143	4.144
	HSE06		2.285	
	Other [6]		0.730	
$AgBaBr_3$				
	GGA-PBEsol	0.817	0.689	0.694
	TB-mBJ	4.410	4.292	4.295
	HSE06		2.174	
	Other [6]		0.640	

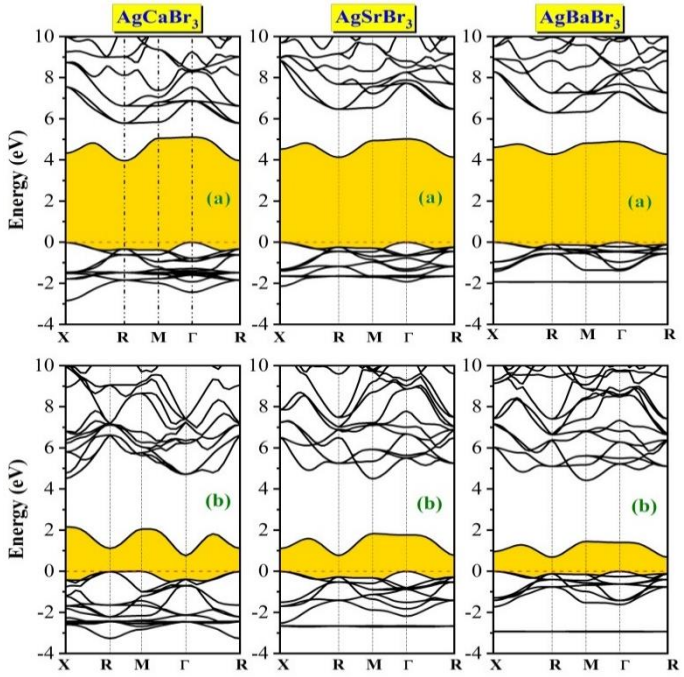

Fig. 6: Band energy dispersions along the high-symmetry directions as calculated using the FP LAPW+lo method with the TB-mBJ (a) and GGA-PBEsol (b) functionals for AgCaBr3, AgSrBr3 and AgBaBr3 materials. The Fermi level is shifted to zero.

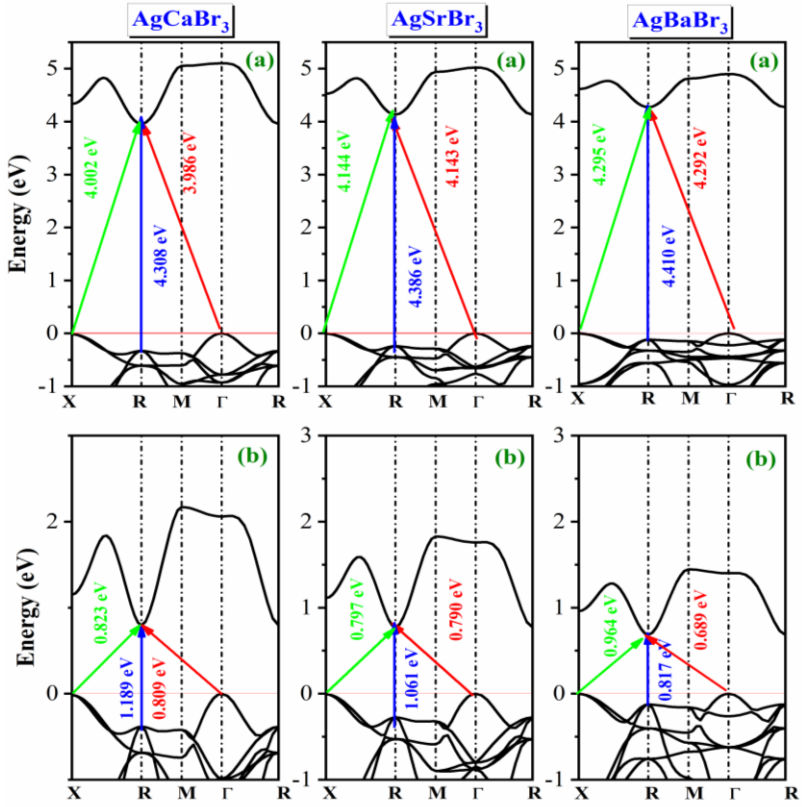

Fig. 7: Enlarged view of the band structure around the fundamental band gap with indication of the values of energy bandgaps Γ–R, R–R and X–R for $AgCaBr_3$, $AgSrBr_3$, and $AgBaBr_3$ materials.

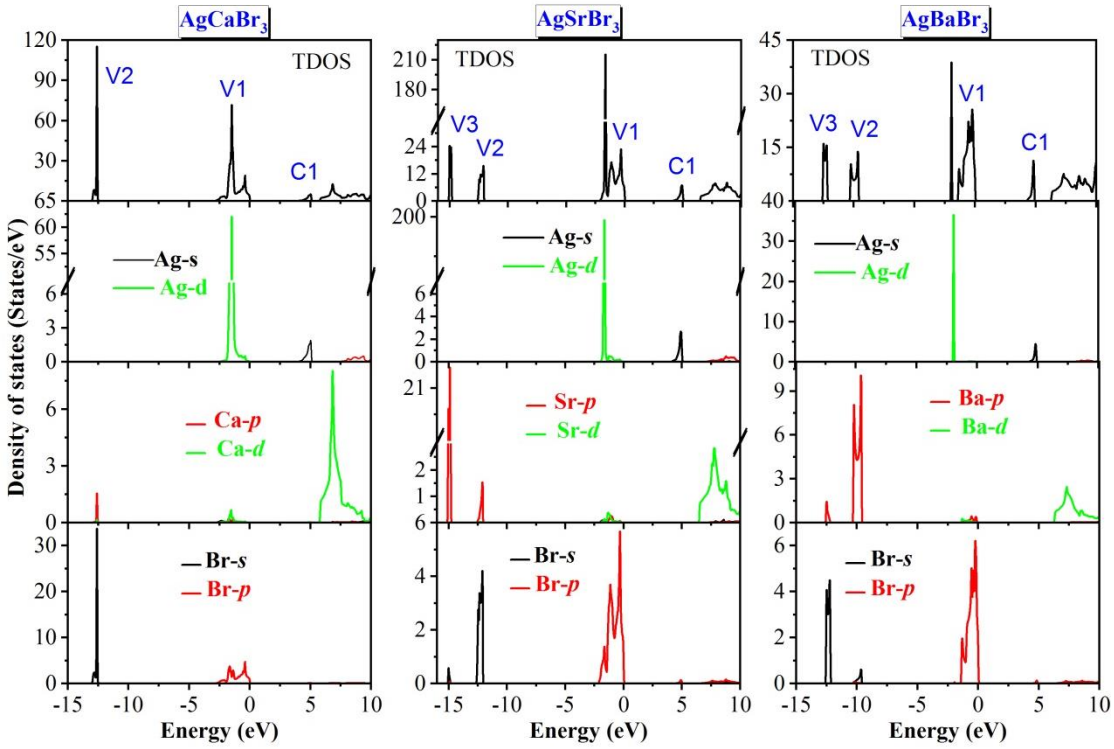

Fig. 8: Total density of state (TDOS) and l-decomposed site projected density of states (PDOS) for $AgCaBr_3$, $AgSrBr_3$, and $AgBaBr_3$ materials as calculated using the TB-mBJ potential. The energy zero (0 eV) is chosen to be at the Fermi energy.

III.2.3 **Optical properties**

An investigation was conducted to examine the optical characteristics of $AgCaBr_3$, $AgSrBr_3$, and $AgBaBr_3$ compounds within the energy range of 0-30 eV. This theoretical investigation was undertaken to analyses the optical properties by examining the frequency-dependent dielectric function, represented as $\varepsilon(\omega) = \varepsilon_1(\omega) + i\varepsilon_2(\omega)$. The absorption events occurring within the crystal are characterized by the imaginary component ($\varepsilon_2(\omega)$) of the dielectric function, which may be determined using the electronic band structure data. The Kramer-Kronig transformation can be used to get the real component ($\varepsilon_1(\omega)$) of the dielectric function, which characterizes the scattering of electromagnetic radiation upon its entry into a medium [27]. The frequency-dependent imaginary and real components of the dielectric function for the materials under investigation are depicted in Fig. 9. The determination of the static dielectric constant occurs at the lower energy limit, which is represented as $\varepsilon(0) = \varepsilon_1(\omega \to 0)$ [28, 29]. The static dielectric constants of $AgCaBr_3$, $AgSrBr_3$, and $AgBaBr_3$

are measured to be 2.88, 2.61, and 2.48, respectively. The findings align with the Penn model [67]: $\varepsilon(0) \approx \hbar\omega_p / E_g^2$, where $\hbar\omega_p$ represents the plasma energy. In other words, a reduction in E_g corresponds to an increase in $\varepsilon(0)$.

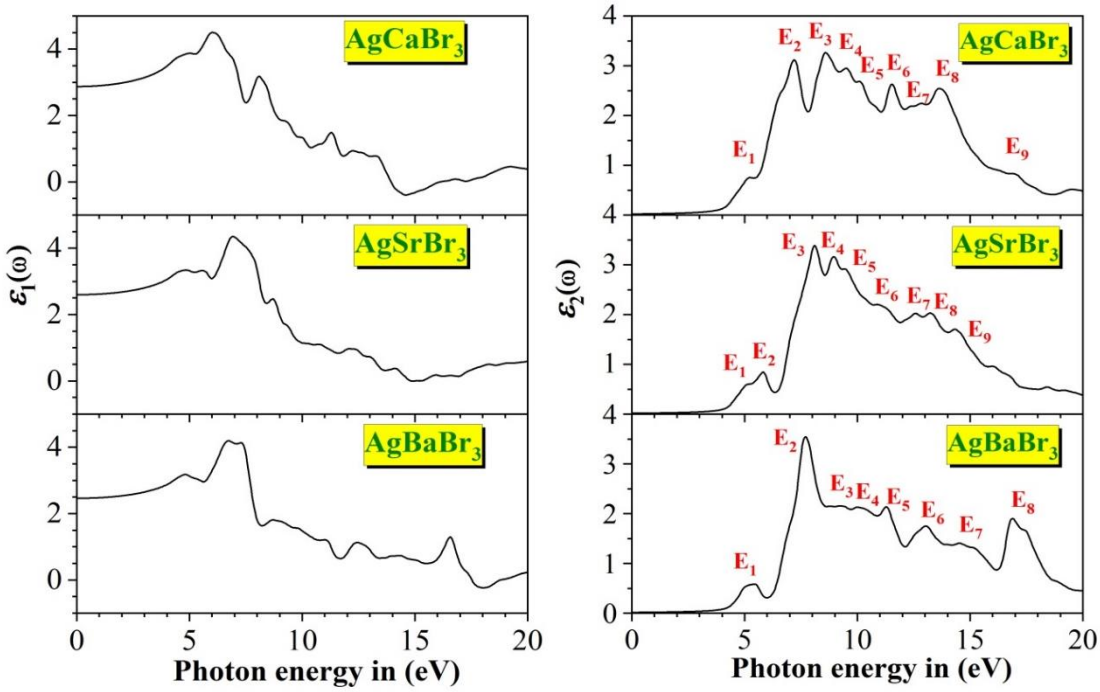

Fig. 9: The spectra of the real ($\varepsilon_1(\omega)$) and imaginary ($\varepsilon_2(\omega)$) parts of the dielectric function for $AgCaBr_3$, $AgSrBr_3$, and $AgBaBr_3$ compounds. The calculations were performed using the TB-mBJ potential.

Fig. 10 displays the spectra of the absorption coefficients α(ω), refractive index n(ω), extinction coefficient k(ω), electron energy loss L(ω), and reflectivity R(ω) for the materials $AgCaBr_3$, $AgSrBr_3$, and $AgBaBr_3$, as functions of incident photon energy. A significant absorption is seen throughout a broad energy range spanning from approximately 3.9 to 42 eV for $AgCaBr_3$, 4.16 to 41 eV for AgSrBr3, and 4.11 to 40.7 eV for $AgBaBr_3$. The compounds $AgCaBr_3$, $AgSrBr_3$ and $AgBaBr_3$ exhibit maximum absorption intensities at approximately 27.1 eV, 22.8 eV and 17.7 eV, respectively. These compounds possess the ability to absorb light within the ultraviolet range and demonstrate transparency within the visible spectrum. As a result, they may serve as efficient filters for a wide array of radiation intensities, encompassing the ultraviolet (UV) spectrum. At energy levels above 42 eV, the transparency of these compounds is observed as a result of a gradual decline in electron reactivity.

The refractive index n(ω) is an essential optical parameter that quantifies the degree of bending of electromagnetic radiation in a given medium [30]. The n(ω) curve exhibits a consistent trend at lower energy levels, progressively rising as energy near the absorption edge, reaching its highest point before decreasing at higher energy levels. The greatest refractive index values observed for $AgCaBr_3$, $AgSrBr_3$, and $AgBaBr_3$ are 2.14, 2.09, and 2.11, respectively, when exposed to photons of energy levels of 6.11 eV, 7.39 eV, and 7.45 eV, respectively. The static refractive index n(0) of $AgCaBr_3$, $AgSrBr_3$, and $AgBaBr_3$ demonstrates an upward tendency, in contrast to the decreasing behavior of the bandgap. In addition, it is worth noting that each compound exhibits distinct energy levels at which the extinction coefficient k(ω) reaches its highest value. Specifically, $AgCaBr_3$ exhibits a peak value of 1.11 at 13.87 eV, $AgSrBr_3$ reaches a peak value of 0.95 at 9.58 eV, and $AgBaBr_3$ reaches a peak value of 0.96 at 7.88 eV.

The materials under consideration have a markedly low static optical reflectivity, with values of 6.7% for $AgCaBr_3$, 5.3% for $AgSrBr_3$, and 4.6% for $AgBaBr_3$. The electron energy loss function (L(ω)) is essential for comprehending the dissipation of energy when high-velocity electrons move through a substance [31]. The L(ω) spectra of $AgCaBr_3$, $AgSrBr_3$ and $AgBaBr_3$ compounds exhibit plasmon peaks at approximately 27.79 eV, 24.09 eV and 19.45 eV, respectively.

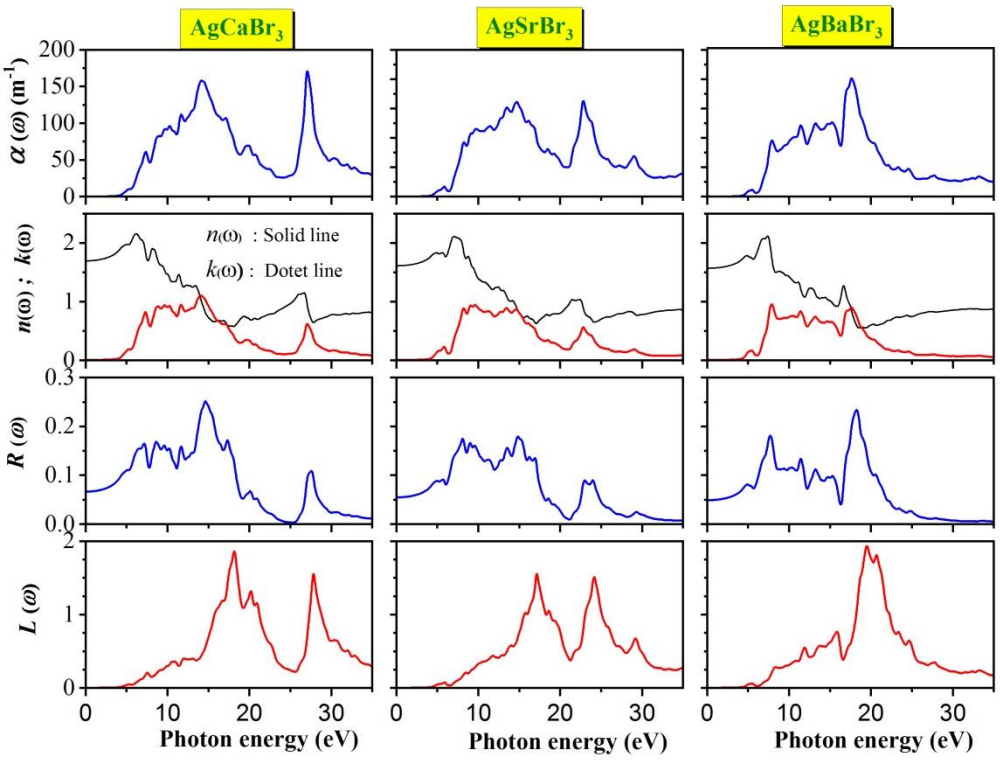

Fig. 10: The calculated spectra of the absorption coefficient α(*ω*), refractive index n(*ω*), extinction coefficient k(*ω*), optical reflectivity R(*ω*) and electron energy loss function L(ω) for AgCaBr3, AgSrBr3 and AgBaBr3 compounds as calculated using the TB-mBJ potential.

Reference:

[1] S.J. Clark, M.D. Segall, C.J. Pickard, P.J. Hasnip, M.J. Probert, K. Refson, M.C. Payne, Zeitschrift fuer Kristallographie 220 (2005) 567.

[2] J.P. Perdew, S. Burke, M. Ernzerhof, Phys. Rev. Lett. 77 (1996) 3865.

[3] D. Vanderbilt, Phys. Rev. B 41 (1990) 7892.

[4] H.J. Monkhorst, J.D. Pack, Phys. Rev. B 13 (1976) 5188.

[5] T.H. Fischer, J. Almlof, J. Phys. Chem. 96 (1992) 9768

[6] J I Gómez-Peralta and X Bokhimi Mater. Chem. Phys. 267 124710 (2021).

[7] F D Murnaghan Proc. Natl. Acad. Sci. 30 244 (1944).

[8] C Li, X Lu, W Ding, L Feng, Y Gao, and Z Guo Acta Crystallogr. B 64 702 (2008).

[9] Y Pan and F Yang J. Energy Storage 87 111492 (2024).

[10] Y Pan Inorg. Chem. 63 8264 (2024).

[11] Y Pan, Z Yang, and H Zhang Int. J. Hydrog. Energy 82 1308 (2024).

[12] J Zhu and Y Pan Mater. Sci. Eng. B 308 117554 (2024).

[13] Y Pan and M Wen J. Am. Ceram. Soc. 107 1081 (2024).

[14] M D Segall, P J Lindan, M al Probert, C J Pickard, P J Hasnip, S J Clark, and M C Payne J. Phys. Condens. Matter 14 2717 (2002).

[15] D V Suetin and I R Shein Phys. Solid State 60 213 (2018).

[16] C-Y Yoo, K-P Hong, and S-J Kim Acta Crystallogr. C 63 i63 (2007).

[17] Y Pan Int. J. Refract. Met. Hard Mater. 121 106676 (2024).

[18] Y Pan Mater. Today Chem. 35 101915 (2024).

[19] Y Pan and F Yang Ceram. Int. 50 14856 (2024).

[20] Y Pan and J Zhu Mater. Today Commun. 38 108428 (2024).

[21] Y Pan and J Zhu Vacuum 225 113242 (2024).

[22] A Gherriche, A Bouhemadou, Y Al-Douri, S Binomran, R Khenata, and M Hadi Mater. Sci. Semicond. Process. 131 105890 (2021).

[23] K Omri, I Najeh, and L El Mir Ceram. Int. 42 8940 (2016).

[24] K Omri, I Najeh, S Mnefgui, N Alonizan, and S Gouadria Mater. Sci. Eng. B 297 116738 (2023).

[25] K Omri, A Bettaibi, K Khirouni, and L El Mir Phys. B Condens. Matter 537 167 (2018).

[26] K Omri and N Alonizan J. Mater. Sci. Mater. Electron. 33 15448 (2022).

[27] A Bouhemadou, S Bin-Omran, D Allali, S M Al-Otaibi, R Khenata, Y Al-Douri, M Chegaar, and A H Reshak Mater. Res. Bull. 64 337 (2015).

[28] A Bouhemadou, S Al-Essa, D Allali, M A Ghebouli, and S Bin-Omran Solid State Sci. 20 127 (2013).

[29] D R Penn Phys. Rev. 128 2093 (1962).

[30] C A Mead Phys. Rev. 128 2088 (1962).

[31] D Allali, A Bouhemadou, E M A Al Safi, S Bin-Omran, M Chegaar, R Khenata, and A H Reshak Phys. B Condens. Matter 443 24 (2014).

GENERAL CONCLUSION

General Conclusion

The present study employed the full potential augmented plane wave plus local orbitals approach to examine the structural, electronic and optical characteristics of the cubic perovskite $AgXBr_3$, where X is Ca, Sr, or Ba. The exchange-correlation interactions were described using three different functionals, specifically GGA-PBEsol, TB-mBJ and HSE06. The results of our study indicate that all three materials demonstrate semiconducting properties. $AgCaBr_3$, $AgSrBr_3$, and $AgBaBr_3$ have an indirect bandgap located between the Γ and R points in BZ. The bandgap values of $AgCaBr_3$, $AgSrBr_3$, and $AgBaBr_3$ using the TB-mBJ (HSE06, GGA PBEsol) functional are 3.986 (2.321, 0.809), 4.143 (2.321, 0.790), and 4.292 (2.174, 0.689) eV, respectively. Calculations of dielectric functions and their associated optical characteristics, such as extinction coefficient, refractive index, absorption coefficient, electronic energy loss function, and reflectivity, have been performed over a broad energy spectrum from 0 to 35 eV. Significant absorption is observed across a broad energy range spanning from approximately 3.9 to 42 eV for AgCaBr3, 4.16 to 41 eV AgSrBr3, and 4.11 to 40.7 eV AgBaBr3. Accordingly, these compounds are capable of absorbing light in the ultraviolet range while maintaining transparency in the visible spectrum. Consequently, they function as effective filter for a wide array of radiation intensities, encompassing the far ultraviolet (UV) spectrum. Additionally, valuable insights into the microscopic origins of the properties of optical spectra were achieved by decomposing the imaginary part of the dielectric function into contributions of different band-to-band transitions and developing transition band structures. Moreover, this methodology facilitated the distinction of contributions originating from various places inside the Brillouin zone. Notably, a rise in the value of the static dielectric constant ε (0) was seen when the bandgap (Eg) decreased, aligning with the predictions made by the Penn model.